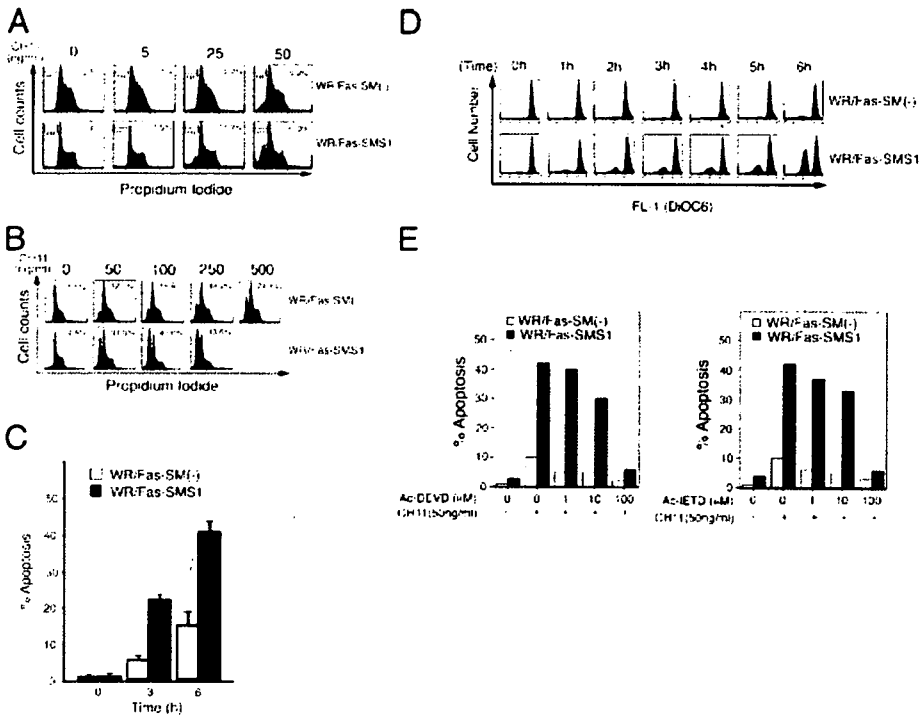

Figure 2. Fas-mediated apoptosis in WR/Fas-SM(−) and WR/Fas-SMS1 cells. (A and B) Dose dependency of Fas-mediated apoptosis. Cells were incubated for 3 h with the indicated concentration of CH11. After incubation, cells were harvested and analyzed by flow cytometry for DNA fragmentation using nuclear staining with PI. The numbers in each box represent the percentages of apoptotic cells. (C) Time kinetics of Fas-mediated apoptosis. Cells were incubated with 50 ng/ml of CH11 for the indicated time, and apoptosis was analyzed by flow cytometry using PI. Error bars represent SEM. (D) Time-kinetics of loss of $\Delta\Psi$m in apoptotic cells. Cells were incubated with 50 ng/ml of CH11 for the indicated time. $\Delta\Psi$m was determined by intracellular staining with $DiOC_6(3)$ and flow cytometry. (E) Inhibition of Fas-mediated apoptosis by caspase inhibitors. Cells were stimulated with 50 ng/ml of CH11 for 6 h in the presence of the indicated amounts of Ac-DEVD-CHO or Ac-IETD-CHO. After incubation, apoptosis was analyzed by flow cytometry using PI.

plays an important role in Fas-mediated apoptosis. Because high antibody concentrations might cause Fas clustering (7), we determined the optimal conditions for Fas-mediated apoptosis by analyzing the effect of concentration of agonistic CH11 (mouse IgM) and the time course of response of these cells. WR/Fas-SMS1 cells underwent stronger apoptosis at 50 ng/ml CH11 than WR/Fas-SM(−) cells, exhibiting 31 and 9.9% apoptosis, respectively (Fig. 2 A). Although apoptosis was increased in a dose-dependent manner in both cells, high concentrations of CH11 (up to 500 ng/ml) induced only 24.3% apoptosis in WR/SMS(−) cells (Fig. 2 B). In subsequent experiments, cells were treated with 50 ng/ml of CH11 as the optimum condition for apoptosis. Next, cells were stimulated with 50 ng/ml CH11 for the indicated time, and WR/Fas-SMS1 cells showed stronger apoptosis compared with WR/Fas-SM(−) cells at both 3 and 6 h (Fig. 2 C).

$\Delta\Psi$m during apoptosis is likely to contribute to the death of the cell through the loss of mitochondrial function before DNA fragmentation in both type I and II cell apoptosis. As shown in Fig. 2 D, the treatment of WR/Fas-SMS1 cells with CH11 dramatically induced a loss of $\Delta\Psi$m as determined by staining with $DiOC_6(3)$, a dye taken up by mitochondria, with similar time kinetics as Fas-mediated apoptosis. However, A majority of WR/Fas-SM(−) cells exhibited a normal $\Delta\Psi$m through the assay (Fig. 2 D). The time kinetics of loss of $\Delta\Psi$m were comparable to those of apoptosis.

Next, we examined whether Fas-mediated apoptosis of WR/Fas-SM(−) and WR/Fas-SMS1 cells depends on caspase activation. Cells were stimulated with 50 ng/ml CH11 for 6 h in the presence of the specific caspase-3 inhibitor (Ac-DEVD-CHO) or the specific caspase-8 inhibitor (Ac-IETD-CHO). As shown in Fig. 2 E, 100 μM of each inhibitor completely suppressed Fas-mediated apoptosis of WR/Fas-SMS1 cells.

Fas-mediated caspase-3 activation of WR/Fas-SM(−) and WR/Fas-SMS1 cells

Cells were stimulated with 50 ng/ml CH11 for the indicated time (Fig. 3 A) and at the indicated concentration for 30 min (Fig. 3 B). Western blot analysis using a caspase-3–specific antibody revealed that the active fragments (p17) of caspase-3 cleaved from 32-kD pro–caspase-3 was expressed at a

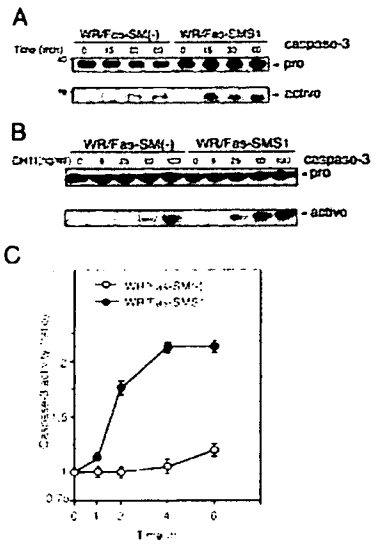

Figure 3. Fas-mediated caspase-3 activation in WR/Fas-SM(−) and WR/Fas-SMS1 cells. Time kinetics (A) and dose dependency (B) of caspase-3 activation by Western blot analysis. Cells were stimulated with 50 ng/ml CH11 for the indicated time (A), or stimulated with the indicated concentration of CH11 for 15 min (B). Total cell lysates were analyzed by Western blot using mouse mAb to caspase-3. The arrows indicate the bands corresponding to 32 kD for procaspase-3 (pro) and 17 kD for the active caspase (active). (C) Cells were stimulated with 50 ng/ml CH11 for the indicated time, and caspase-3 activities were measured in extracts of cell lysates using colorimetric assay kits. Each experiment was done in triplicate. Data are representative of five independent experiments. Error bars represent SEM.

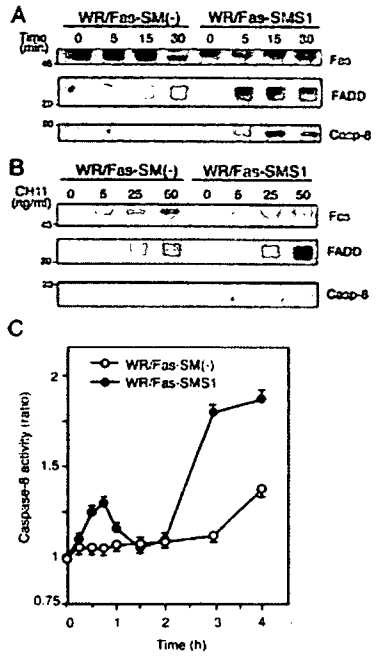

Figure 4. Fas-mediated DISC formation and caspase-8 activation in WR/Fas-SM(−) and WR/Fas-SMS1 cells. Time kinetics (A) and dose dependency (B) of Fas-mediated DISC formation. 2×10^7 cells were stimulated with 50 ng/ml CH11 for the indicated time (A) or stimulated for 15 min with the indicated concentration of CH11 (B). After stimulation, Fas was immunoprecipitated with anti-mouse IgM antibody from Brij 97 lysates. Immunoprecipitates were subjected to 12% SDS-PAGE and immunoblotted with anti-Fas death domain (3D5), anti-FADD, and anti-caspase-8 mAb. Data are representative of five independent experiments. (C) Fas-mediated activation of caspase-8. Cells were stimulated with 50 ng/ml CH11 for the indicated time, and caspase-8 activities were measured in extracts of cell lysates using colorimetric assay kits. Each experiment was done in triplicate. Data are representative of five independent experiments. Error bars represent SEM.

higher level in WR/Fas-SMS1 cells compared with WR/Fas-SM(−) cells in time-dependent (Fig. 3 A) and concentration of Fas antibody–dependent manners (Fig. 3 B). As shown in Fig. 3 C, colorimetric assay revealed that cytoplasmic caspase-3 activity of WR/Fas-SMS1 cells increased more than twofold over baseline by Fas cross-linking. However, caspase-3 activity of WR/Fas-SM(−) cells remained at baseline for the entire 6 h.

Fas-mediated DISC formation and caspase-8 activation in WR/Fas-SM(−) and WR/Fas-SMS1 cells

According to the current model of type I apoptosis, binding of either the FasL or an agonistic antibody induces aggregation of Fas followed by a conformational change in its cytoplasmic domain that results in formation of the DISC (2, 3, 18). Therefore, we examined DISC formation in WR/Fas-SM(−) and WR/Fas-SMS1 cells. Cells were stimulated with 50 ng/ml CH11 for the indicated time (Fig. 4 A) and at the indicated concentration (Fig. 4 B) for 30 min. After lysis, Fas was immunoprecipitated with anti–mouse IgM antibody, and precipitated proteins were examined by immunoblotting with anti-FADD or anti–caspase-8 antibody. The results of the time course study revealed that FADD associated with Fas within 5 min in both cells. However, the association of FADD and Fas in WR/Fas-SMS1 cells was stronger and sooner (with the maximum association at 5 min) than in WR/Fas-SM(−) cells, in which the association gradually increased over the 30-min period. Caspase-8 appeared within the DISC in WR/Fas-SMS1 cells after 5 min of stimulation and reached maximum levels at 15 min. However, caspase-8 within DISC in WR/Fas-SM(−) cells was barely detectable throughout the assay (Fig. 4 A). The results of a dose-dependent experiment revealed that association of FADD and caspase-8 with Fas in WR/Fas-SMS1 cells appeared much stronger than in WR/Fas-SM(−) cells at any concentration of antibody (Fig. 4 B). Although FADD was detected in the DISC after stimulation with 5 ng/ml CH11 in both cell types, caspase-8 appeared in the DISC at a relatively high concentration of CH11; i.e., 25 ng/ml for WR/Fas-SMS1 and 50 ng/ml for WR/Fas-SM(−) cells, respectively (Fig. 4 B).

We also examined the cytoplasmic caspase-8 activity in WR/Fas-SM(−) and WR/Fas-SMS1 cells after Fas cross-linking by colorimetric assay. Interestingly, caspase-8 activities in WR/Fas-SMS1 cells exhibited a biphasic peak after stimulation: the first small peak appeared within 1 h; and the second high peak, after 2 h. However, caspase-8 activity in WR/Fas-SM(−) cells remained at baseline for 3 h, with slight increase at 4 h (Fig. 4 C).

Fas aggregation and capping in WR/Fas-SM(−) and WR/Fas-SMS1 cells

It has been reported that Fas, as well as TNFR, assemble into trimers in the absence of ligands (19, 20). Although Fas trimers do not trigger apoptosis in the resting condition, clustering of these trimers is crucial for Fas-mediated apoptosis (18, 21). CH11 causes the formation of Fas multimers, thereby inducing complete cellular activation leading to capping. Kamitani et al. reported that cross-linking of Fas on the cell surface by CH11 resulted in the formation of high molecular mass Fas aggregates, which were stable in 2% SDS and 5% β-mercaptoethanol (22). As shown in Fig. 5, stimulation with CH11 induced the formation of SDS- and 2-ME–stable, high molecular aggregates (>200 kD) of Fas in both cells, as reported by others (22, 23). Fas aggregates appeared more strongly in WR/Fas-SMS1 cells compared with WR/Fas-SM(−) cells in time-dependent (Fig. 5 A) and CH11 dose–dependent (Fig. 5 B) fashions.

We used confocal microscopy to examine Fas capping on the plasma membrane of WR/Fas-SM(−) and WR/Fas-SMS1 cells after treatment with 50 ng/ml CH11 as described in Materials and methods. In unstimulated cells, Fas was diffusely distributed across the surface on both WR/Fas-SM(−) and WR/Fas-SMS1 cells (Fig. 5 C, 0 min). Cross-linking of Fas with antibody induced small patches of Fas along the plasma membrane, which appeared to fuse to large clusters/capping in WR/Fas-SMS1 cells (Fig. 5 C, 30 min). The frequency of Fas capping on WR/Fas-SMS1 cells was significantly greater than that of WR/Fas-SM(−) cells at each time point ($P < 0.01$; Fig. 5 D).

Fas distribution in lipid rafts of WR/Fas-SM(−) and WR/Fas-SMS1 cells

Recent studies have shown that rafts play an important role in signal transduction pathways, including apoptosis and, in particular, through the organization of surface receptors, signaling enzymes, and adaptor molecules into rafts (5, 24). Muppidi et al. have reported that translocation of Fas into lipid rafts increased sensitivity to Fas-mediated apoptosis (25). To determine Fas distribution of WR/Fas-SM(−) and WR/Fas-SMS1 cells, rafts were isolated using equilibrium

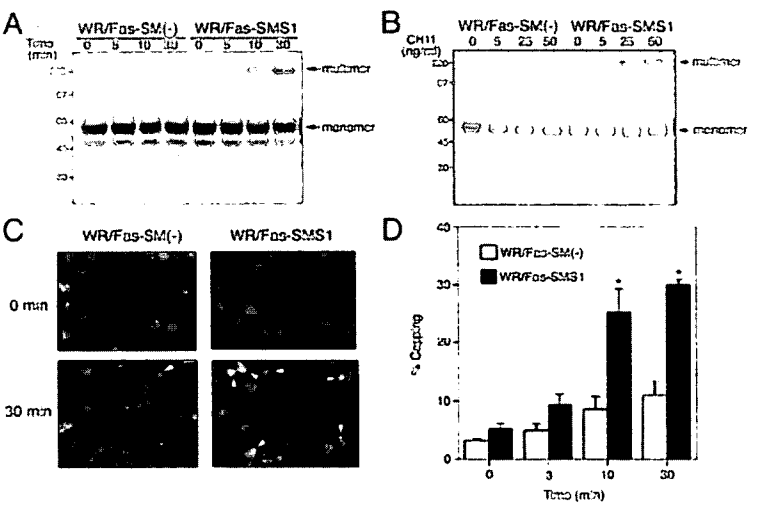

Figure 5. Fas clustering and capping in WR/Fas-SM(−) and WR/Fas-SMS1 cells. Time kinetics (A) and dose dependency (B) of Fas multimer formation. 4×10^7 cells were stimulated with 50 ng/ml CH11 for the indicated time (A), or stimulated for 10 min with the indicated concentration of CH11 (B). After stimulation, cell pellets were snap frozen and treated at 45°C for 1 h in 300 μl of a 1% NP-40–treating solution. DNA in the samples was sheared with a 25-gauge needle, and solubilized samples were loaded on 12% SDS-PAGE. Fas multimers were detected with antibody to the intracellular death domain of human Fas (3D5). Data are representative of more than three independent experiments. (C) Activation-induced capping of Fas. Cells were stained for 20 min with 50 ng/ml CH11 at 4°C. Afterwards, capping was induced by warming cells to 37°C for 30 min in a water bath with mild agitation. Cells were harvested at the indicated times and fixed with 4% paraformaldehyde for 20 min at 22°C. Fixed cells were washed twice and mounted in FITC-conjugated secondary antibody. Fluorescence was detected using a confocal microscope equipped with a SPOT digital camera. The data are representative of more than five experiments. Arrowheads indicate Fas capping. (D) Time kinetics of activation-induced Fas capping. Capping was induced for the indicated time, and cells with Fas clustering were counted by two independent observers. Percentages of capping were calculated in 150–200 total cells. These results are the mean of three independent experiments. Error bars represent SEM. *, $P < 0.01$.

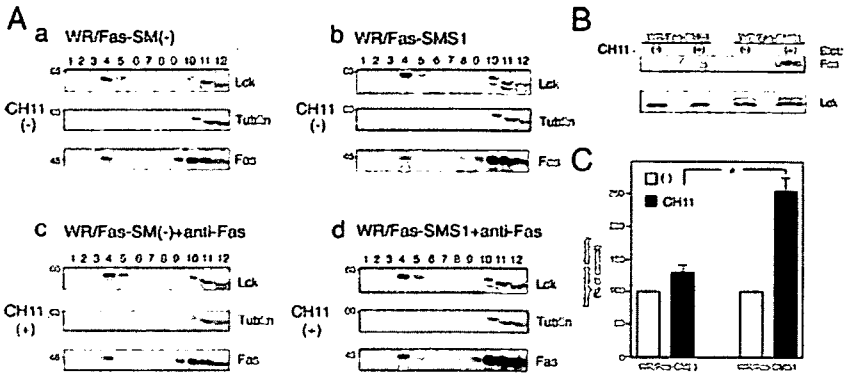

Figure 6. Distribution of Fas into lipid rafts of WR/Fas-SM(−) and WR/Fas-SMS1 cells. (A) 10^5 cells were left unstimulated (a and b) or were stimulated with CH11 for 30 min (c and d), and Triton X-100 lysates were subjected to sucrose density gradient fractionation. Fractions were run on 15% SDS-PAGE and immunoblotted with antibodies against *lck* (a marker for the raft fractions), tublin (a marker for the nonraft fractions), and Fas (3D5). The blots shown are representative of four independent experiments. (B) Redistribution of Fas into lipid rafts on stimulation. Raft fractions (fraction 4) were run on 15% SDS-PAGE and immunoblotted with antibodies against *lck* and Fas. (C) Quantification of Fas contents in lipid rafts was performed densitometrically and normalized to the amount of *lck*. Data are expressed as the mean ± SEM for relative increase of three independent experiments. *, $P < 0.01$.

sucrose density gradients. The position of the membrane rafts in the sucrose gradient was determined by the presence of *lck*, a well-established raft-associated molecule. As shown in Fig. 6, *lck* was enriched in the upper part of the sucrose gradient (fractions 4 and 5), with a secondary localization at the bottom of the gradient in which a cytoskeletal protein, tublin, was localized (fractions 10–12), indicating a separation of the lipid rafts (fractions 4 and 5) from the Triton X-100–soluble membrane. Fas was detected in raft fractions of WR/Fas-SM(−) and WR/Fas-SMS1 cells before stimulation (Fig. 6 A, a and b). Although a substantial shift of Fas into raft fractions was observed in both cells after stimulation, amounts of Fas in raft fractions were greater in WR/Fas-SMS1 than in WR/Fas-SM(−) cells (Fig. 6 A, a and c vs. Fig. 6 A, b and d). The mean of three independent experiments revealed that Fas redistribution in raft fractions was significantly greater in WR/Fas-SMS1 cells than in those of WR/Fas-SM(−) cells after stimulation ($P < 0.01$; Fig. 6, B and C).

Ceramide generation in lipid rafts of WR/Fas-SM(−) and WR/Fas-SMS1 cells

Ceramide modulates the activity of a large number of proteins, and a role in apoptosis induction has been proposed (26–28). However, the signals that activate the enzyme responsible for ceramide production are not well defined, and the actual contribution of ceramide to the apoptotic response remains poorly understood. It has been reported that ceramide formation is associated with the execution phase of apoptosis as a consequence of processes downstream of the activation of caspases (29, 30). Consistent with this, we observed delayed generation of cytosolic ceramide in WR/Fas-SMS1 compared with WR/Fas-SM(−) cells after a 2-h Fas stimulation (unpublished data). However, stress-induced SM hydrolysis occurs rapidly, suggesting that the early event is located in close proximity to the plasma membrane. Recently, it has been reported that aSMase translocates into rafts within minutes after cell stimulation and catalyzes the formation of ceramide from SM (11, 31, 32). Therefore, we analyzed membrane ceramide within lipid rafts in WR/Fas-SM(−) and WR/Fas-SMS1 cells. Although WR/Fas-SM(−) cells, because of a lack of SM synthase, contain more ceramide than WR/Fas-SMS1 cells, both cells showed a similar distribution of ceramide among fractions (Fig. 7 A). Thus, in both cell types, 70% of ceramide is located in raft fractions with ~40% in fraction 4 (Fig. 7 A, bottom). Because membrane SM is one of the major sources of ceramide generation, we next examined Fas-stimulated ceramide generation in raft fractions of WR/Fas-SM(−) and WR/Fas-SMS1 cells. After 5 min of Fas stimulation, cells were lysed, and rafts were isolated using equilibrium sucrose density gradients. Analysis of ceramide in the raft fraction revealed that Fas cross-linking increased ceramide content by 50% in WR/Fas-SMS1 cells (from 2,955 to 4,386 pmol/10^6 cells), but marginally decreased ceramide in WR/Fas-SM(−) cells (from 5,960 to 5,651 pmol/10^6 cells; Fig. 7 B). The mean of three independent experiments revealed that ceramide contents of raft fractions in WR/Fas-SMS1 cells were significantly greater than those of WR/Fas-SM(−) cells ($P < 0.01$; Fig. 7 C).

Effects of exogenous ceramide on Fas-mediated apoptosis in WR/Fas-SM(−) and WR/Fas-SMS1 cells

We and others have shown that ceramide is a proapoptotic lipid mediator because diverse mechanisms of cell stress, including CH11 cross-linking, TNF-α treatment, irradiation, heat shock, and anticancer drugs, increases intracellular ceramide during the execution phase of apoptosis (27, 28, 31, 33–37). It has been reported that the addition of natural or

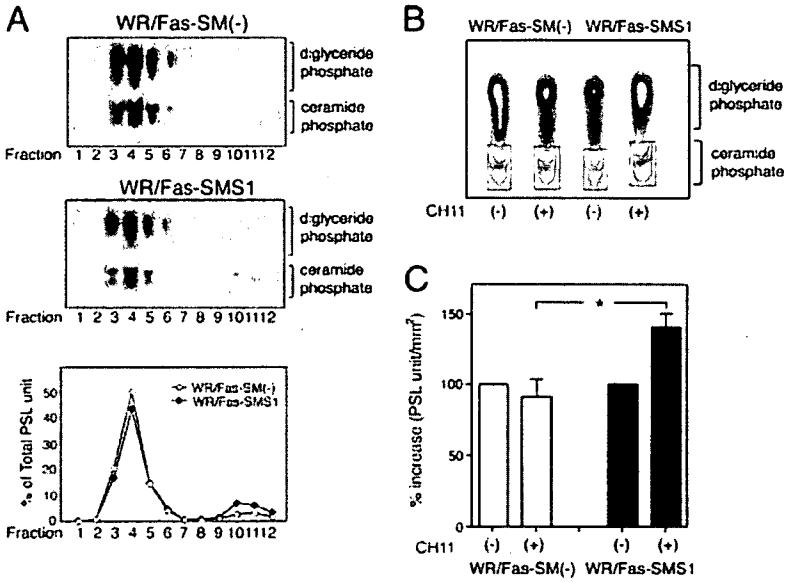

Figure 7. Ceramide generation in lipid rafts of WR/Fas-SM(−) and WR/Fas-SMS1 cells. (A) Ceramide contents in membrane fractions of sucrose density gradient fractionation. 10^8 cells were lysed in Triton X-100 buffer and subjected to sucrose density gradient fractionation. Lipids of each fraction were extracted by the method of Bligh and Dyer (reference 53), and ceramide content was measured by the diacylglycerol kinase assay. After separation of ceramide-1-phosphates by TLC, radioactivity was visualized and estimated. The results are representative of three independent experiments and expressed as the percentage of total PSL arbitrary units. (B) Fas-mediated ceramide generation in lipid rafts. 10^8 cells were left unstimulated or were stimulated with CH11 for 5 min and Triton X-100 lysates were subjected to sucrose density gradient fractionation. Lipids of raft fraction (fraction 4) were extracted by the method of Bligh and Dyer, and ceramide generation was measured by the diacylglycerol kinase assay. Radioactivity was visualized and estimated. The results are representative of three independent experiments. (C) The mean of three independent experiments revealed that ceramide contents of lipid rafts in WR/Fas-SMS1 cells were significantly greater than those of WR/Fas-SM(−) cells. The results were the mean of three independent experiments and expressed as the percentage increase of PSL arbitrary units. Error bars represent SEM. *, $P < 0.01$.

C16-ceramide, which by themselves did not induce apoptosis, enabled soluble FasL to cap and completely restore the apoptosis in aSMase$^{-/-}$ hepatocytes (10, 11, 38). Therefore, we examined the effects of exogenous natural or C16-ceramide on Fas-mediated apoptosis and the formation of Fas multimers in WR/Fas-SM(−) and WR/Fas-SMS1 cells. Cells were pretreated with the indicated concentration of natural or C16-ceramide for 1 h. After washing, cells were stimulated with 50 ng/ml of agonist CH11 for 6 h before assaying for apoptosis, or 30 min before assessing Fas multimer formation. Although natural and C16-ceramide did not induce apoptosis by themselves, both ceramides enhanced Fas-induced apoptosis. However, high concentrations of ceramides, even at 5 μM, could not restore apoptosis of WR/Fas-SM(−) cells to the levels of WR/Fas-SMS1 cells (Fig. 8, A and B). We also examined the effects of natural or C16-ceramide on Fas multimer formation and found that pretreatment of cells with 5 μM natural or C16-ceramides did not enhance Fas multimer formation in WR/Fas-SM(−) and WR/Fas-SMS1 cells (unpublished data).

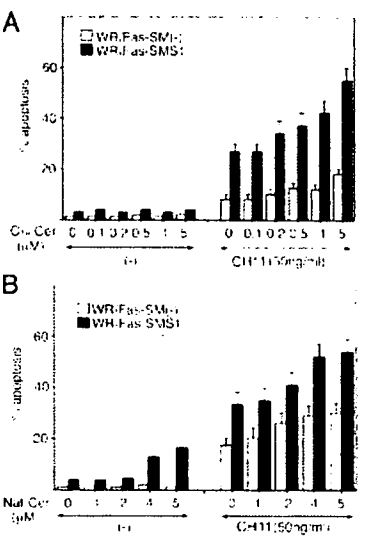

Figure 8. Effects of exogenous ceramides on Fas-mediated apoptosis in WR/Fas-SM(−) and WR/Fas-SMS1 cells. Cells were pretreated with the indicated concentration of C16- (A) or natural (B) ceramide for 1 h. After washing, cells were stimulated with 50 ng/ml CH11 for 6 h and apoptosis was analyzed by flow cytometry using PI. Error bars represent SEM.

DISCUSSION

Currently, two distinct pathways are proposed in Fas-mediated apoptosis signaling; i.e., type I and type II apoptosis. The

consensus in type I apoptosis is that FasL, itself a homotrimer, engages three Fas monomers, leading to the assembly of a trimeric Fas receptor. This FasL-induced trimerization has been suggested to bring together death domains present in the cytoplasmic region of each Fas monomer, leading to a DISC formation. However, it has been reported that soluble FasL (sFasL) reduced apoptosis by <1,000-fold compared with membrane-bound FasL (39), and that sFasL or antibodies to Fas cause cell death more efficiently if polymerized by adsorption on plastic or by molecular cross-linking (40), suggesting that clustering of Fas is important in Fas-mediated apoptosis. Recently, Fas, as well as TNFR, has been reported to assemble into trimers in the absence of ligands through a preligand assembly domain in the extracellular, amino-terminal region of receptors (19, 41). Moreover, Siegel et al. showed that Fas trimers in the absence of FasL do not recruit the DISC, implying a lack of apoptotic signaling (19). Thus, it has been believed that the oligomerization of preassembled Fas trimers is essential for optimal acute signaling and direct activation of the caspase cascade through the DISC (18, 21). However, the molecular basis of Fas clustering is not clear.

It has been reported that Fas ligation triggers translocation of aSMase from an intracellular compartment onto the cell surface, where it hydrolyzes SM to ceramide, and that accumulation of ceramide contributes to transforming small rafts into larger aggregates for signaling platforms, which trap and cluster Fas (7, 10, 11, 31, 42). In contrast to the extensive studies of the acid or neutral SMase in cell death, the biological function of SM synthase has not been elucidated because of a lack of molecular cloning of its responsible genes. Recently, we have succeeded in cloning *SMS1* (12) and established WR/Fas-SM(−) and WR/Fas-SMS1 cells (Fig. 1). Using this system to investigate the mechanisms of Fas-mediated apoptosis, we report here that restoration of membrane SM by transfection of SM synthase gene into SM-deficient cells restored Fas-mediated apoptosis (Fig. 2) through DISC formation (Fig. 4, A and B), activation of caspase-3 (Fig. 3) and caspase-8 (Fig. 4 C), and Fas clustering (Fig. 5). The equivalent expression of other lipid components in the plasma membrane, such as ganglioside GM1 and cholesterol (Fig. 1 C), and equivalent localization of raft fractions in sucrose density gradients (Fig. 6) argue against other lipid abnormalities in SM-deficient cells.

Because lipid rafts promote efficient formation of receptor-associated signaling complexes to produce the biological outcomes dictated by these complexes (24, 43–45), redistribution of Fas in lipid rafts is one possible mechanism for regulating the efficiency of Fas signaling. After titration of Triton X-100 for the isolation of lipid rafts (Fig. S1, available at http://www.jem.org/cgi/content/full/jem.20041685/DC1), we examined whether the redistribution of Fas in lipid rafts is different between WR/Fas-SM(−) and WR/Fas-SMS1 cells. Although Fas cross-linking enhanced redistribution of Fas into raft fractions in both cells, Fas contents in raft fractions were greater in WR/Fas-SMS1 than WR/Fas-SM(−) cells (Fig. 6). These results suggest that membrane SM plays a crucial role for raft partitioning of Fas, which is one of the important mechanisms in Fas-mediated apoptosis of these cells.

It has been believed that the trapping and clustering of Fas may promote the formation of multimers, which ultimately transmit a strong signal into the cell that induces apoptosis (18, 21). We examined the efficiency of Fas clustering in WR/Fas-SM(−) and WR/Fas-SMS1 cells and found that the aggregation and clustering of Fas in WR/Fas-SMS1 cells were markedly enhanced after Fas cross-linking compared with that in WR/Fas-SM(−) cells (Fig. 5), suggesting that oligomerization of Fas is crucial for optimal apoptosis signaling. Although the exact mechanisms of platform formation for Fas clustering on the membrane are not clear, it has been reported that aSMase translocates from an intracellular compartment to the extracellular surface of the cell membrane on Fas stimulation, and that translocation of aSMase to SM-rich rafts generates ceramide (11, 42). Therefore, using a diacylglycerol kinase assay, we measured ceramide content in raft fractions of WR/Fas-SM(−) and WR/Fas-SMS1 cells before and after Fas stimulation. Although ceramide generation in WR/Fas-SM(−) cells is not increased by Fas cross-linking, WR/Fas-SMS1 cells showed a 50% increase in ceramide contents in a raft fraction within 5 min after Fas stimulation (Fig. 7). Because it has been reported that ceramide displaces cholesterol from lipid rafts (46) and self-associates within lipid rafts through hydrogen bonding (47), ceramide may provide the driving force that results in the coalescence of microscopic rafts into large-membrane macrodomains (48), indicating that ceramide in rafts serves to form a signaling platform for Fas clustering (7, 49).

Ceramide has been recognized as an important intracellular lipid mediator related to a variety of cell functions, including cell differentiation and apoptosis (27, 28, 31, 33–37, 50). It has also been reported that the addition of exogenous natural or C16-ceramide enabled soluble FasL to cap and completely restored the apoptosis in aSMase$^{-/-}$ hepatocytes (10, 11, 38). Although exogenous ceramides partially enhanced Fas-mediated apoptosis, they could neither restore apoptosis nor enhance Fas multimer formation in WR/Fas-SM(−) cells to the levels in WR/Fas-SMS1 cells (Fig. 8). In this regard, Liu et al. have reported that IL-1β induced the loss of a resident population of SMs from the SM-rich plasma membrane (i.e., lipid rafts) and the concomitant appearance of ceramide (51). Therefore, we hypothesize that intact SM-enriched membrane domains may be essential for local ceramide production that compartmentalize lipid rafts to ceramide-enriched membrane platforms, leading to Fas capping.

Concerning the molecular ordering of the initial signaling events of CD95, Algeciras-Schimnich et al. have reported four stages: (a) ligand-induced formation of CD95 microaggregates at the cell surface; (b) recruitment of FADD to form a DISC; (c) formation of large CD95 surface clusters, which is positively regulated by DISC-generated caspase-8; and (d)

internalization of activated CD95 through an endosomal pathway (52). We examined caspase-8 activation, ceramide generation within lipid rafts, redistribution of Fas within lipid rafts, and Fas multimer formation at very early time points (Fig. S2, available at http://www.jem.org/cgi/content/full/jem.20041685/DC1). Caspase-8 activation, ceramide generation, and Fas redistribution within lipid rafts were observed within 1 min in WR/Fas-SMS1 but not WR/Fas-SM(−) cells. In contrast, Fas multimer formation was observed in WR/Fas-SMS1 but not WR/Fas-SM(−) cells at later time points (after 2 min; Fig. S2). Thus, our findings support a crucial role for membrane SM in the extrinsic pathway of Fas-mediated apoptosis through the generation of ceramide in lipid rafts, which facilitates efficient Fas clustering, DISC formation, and the early caspase-8 activation leading to the downstream cascade of caspase-3 activation.

MATERIALS AND METHODS

Cells and cell transfection. Mouse T cell lymphoma WR19L cells transfected with the cDNA for the human *Fas* gene (WR19L/Fas; reference 15) were a gift of S. Yonehara (Kyoto University, Kyoto, Japan). We isolated the SM-defective WR/Fas-SM(−) cells and the SM-containing WR/Fas-SM(+) cells from the original WR19L/Fas cells by limiting dilution. *SMS1*, subcloned into the pLIB expression vector, was transfected into the WR/Fas-SM(−) cells in VSV-G retroviral particles. These cells were designated WR/Fas-SMS1 cells (12).

Antibodies and reagents. Anti-Fas (CH11, mouse IgM) and anti-FADD (1F7, mouse IgG1) were purchased from MBL International Corporation. FITC-conjugated anti-mouse IgM, anti-mouse IgG2a, anti-human Fas (DX2), and anti-caspase-3/CPP32 pAb were purchased from BD Biosciences. Anti-Fas death domain (3D5) and anti-caspase-8 (1G12) antibodies were purchased from Qbiogene. Lysenin, FITC-conjugated CTx, peroxidase-conjugated CTx, and methyl-β-cyclodextrin were purchased from Sigma-Aldrich. Rabbit anti-mouse IgG mAb was purchased from Cappel. Ac-DEVD-CHO and Ac-IETD-CHO were purchased from Peptide Institute. RNase and saponin were purchased from Nacalai Tesque. The cell viability assay kit using WST-8 (2-(2-methoxy-4-nitrophenyl)-3-(4-nitrophenyl)-5-(2,4-disulfophenyl)-2H-tetrazolium) was purchased from Wako Co. Ltd. L-[^{14}C]serine and γ-[^{32}P]ATP were purchased from GE Healthcare. Rabbit anti-mouse IgM (μ chain specific) antibody was purchased from Zymed Laboratories. The ECL immunodetection system and horseradish peroxidase–conjugated goat anti-mouse or anti-rabbit IgG mAb were obtained from GE Healthcare.

FACS analysis. DNA fragmentation was quantified by analyzing cell cycle and total DNA content to measure cell death by apoptosis. In brief, cells were treated with CH11 at the indicated concentration and incubated for the indicated time shown in the figures. After harvesting, cells were resuspended in permeabilization solution (0.5% paraformaldehyde and 0.5% saponin) and treated with 50 μg/ml RNase A for 30 min at room temperature, and propidium iodide (PI; Molecular Probes) was added to a final concentration of 20 μg/ml. After 20 min, the fluorescence of the PI-stained DNA was quantitated on a per cell basis using a FACSCalibur (BD Biosciences), and cells with subdiploid content were considered to be apoptotic cells.

To detect SM localized at the outer leaflet of the plasma membrane, cells were stained on ice for 30 min with nontoxic lysenin–MBP (16), incubated for 30 min with FITC-conjugated anti-mouse IgG (Sigma-Aldrich), and analyzed with a FACSCalibur. Surface expression of ganglioside GM1 and cholesterol was analyzed using FITC-conjugated CTx) or fPEG-cholesterol (17), respectively. Data were analyzed using CellQuest software (Becton Dickinson).

To assess ΔΨm, healthy or dying cells were incubated for 15 min at 37°C in buffer containing 40 nM 3,3′-dihexyloxacarbocyanine iodide ($DiOC_6(3)$; Molecular Probes) before the addition of 5 μg/ml PI. After compensation to exclude nonviable cells, fluorescence was recorded at 525 nM (FL-1) for $DiOC_6(3)$ and 600 nM (FL-3) for PI on a FACScan (26).

Confocal microscopy. To assess Fas capping, cells were stained for 20 min with 50 ng/ml of CH11 at 4°C, and capping was induced by warming cells to 37°C in a water bath with mild agitation. Cells were harvested at the indicated times shown in the figures and fixed with 4% paraformaldehyde for 10 min at 22°C. Fixed cells were washed twice and mounted in FITC-conjugated secondary antibody. Fluorescence was detected with a confocal microscope (LSM-5 Pascal; Carl Zeiss MicroImaging, Inc.) equipped with a SPOT digital camera. Large clusters of Fas were defined as cells in which the fluorescence condenses onto >25% of the cell surface, whereas fluorescence was homogeneously distributed on the membrane of resting cells.

For visualization of SM localized at the outer leaflet of the plasma membrane, cells were allowed to settle onto slides coated with poly-L-lysine, fixed in 4% formaldehyde, stained with lysenin–MBP at 4°C for 45 min, and treated with anti-MBP.

Cell labeling and lipid separation. The method for detection of SM synthesis is described elsewhere (28). In brief, cells were reseeded at 5×10^5 cells/ml in RPMI 1640 with 2% FBS and L-[^{14}C]serine (specific activity, 155 mCi/mmol) and incubated at 37°C in 5% CO_2 for 36 h. The cell lipids were extracted by the method of Bligh and Dyer (53), applied on silica gel TLC plate (Whatman), and developed with solvent containing methyl acetate/propanol/chloroform/methanol/0.25% KCl (25:25:25:10:9). The radioactive spots were visualized and quantified using an image analyzer (BAS 2000; Fuji Photo Film).

Immunoprecipitation, Western blotting, and immunoblotting. Cells were solubilized with lysis buffer containing 50 mM Tris-HCl, pH 7.6, 1% Brij 97, 300 mM NaCl, 5 mM EDTA, 10 μg/ml leupeptin, 10 μg/ml aprotinin, 1 mM PMSF, and 1 mM sodium orthovanadate with gentle rocking for 30 min at 4°C. Immunoprecipitated proteins were eluted by boiling in SDS-containing sample buffer and fractionated by SDS-PAGE (8–12% polyacrylamide gels; reference 54). Proteins were electrophoretically transferred to polyvinylidene difluoride (Immobilon-P) membranes (Sigma-Aldrich). Peroxidase-conjugated secondary antibodies (GE Healthcare) were used at a 1:1,000 dilution, and immunoreactive bands were visualized using ECL. Densitometry of the protein bands was performed using National Institutes of Health image software (55). Quantitation of Fas in raft fractions was corrected to the amount of *lck*.

The aggregated form of Fas was detected by the method of Kamitani et al. (22). In brief, cell pellets were snap frozen to prevent protein degradation. Frozen pellets were treated at 45°C for 1 h in 300 ml of 2% treating solution containing 5% β-mercaptoethanol. DNA in the samples were sheared with a 25-gauge needle, and solubilized samples were loaded on 12% SDS-PAGE. Aggregated Fas was detected by 3D5, a mouse mAb (IgG1) specific for the intracellular death domain of human Fas (Qbiogene).

Caspase activity assay. Activities of caspase-3 and -8 were determined using a colorimetric assay kit (MBL International Corporation) according to the manufacturer's protocol. Apoptosis inhibition was assayed in cells stimulated for 6 h with 50 ng/ml CH11 in the presence of the indicated doses of Ac-DEVD-CHO or Ac-IETD-CHO shown in the figures.

Isolation of a raft fraction in equilibrium density gradients. Raft fractions were prepared as described by Rodgers and Rose (56) with minor modifications (8). In brief, 10^8 cells were lysed with 1 ml MS-buffered saline (MBS; 25 mM MES, pH 6.5, and 150 mM NaCl) containing 1% Triton X-100, 10 μg/ml aprotinin, 10 μg/ml leupeptin, 1 mM PMSF, 1 mM sodium orthovanadate, and 5 mM EDTA. The lysate was homogenized

with 20 strokes of a Dounce homogenizer (Iwaki Glass Co.), gently mixed with an equal volume of 80% sucrose (wt/vol) in MBS, and placed in the bottom of a 14 × 95 mm clear centrifuge tube (model 344060; Beckman Coulter). The sample was then overlaid with 6.5 ml of 30% sucrose and 3.5 ml of 5% sucrose in MBS and centrifuged at 200,000 *g* in a rotor (model SW40Ti; Beckman Coulter) at 4°C for 16 h. After centrifugation, 12 1-ml fractions (excluding the pellet) were collected from the top of the gradient.

Ceramide measurement. Lipids were extracted from cell lysates by the method of Bligh and Dyer (53), and ceramide mass measurement using *Escherichia coli* diacylglycerol kinase, which phosphorylates ceramide to ceramide-1-phosphate, was performed as described previously (50). The solvent system to separate ceramide-1-phosphate and phosphatidic acid on TLC plates consists of chloroform/acetone/methanol/acetic acid/H_2O (10:4:3:2:1). Radioactivity within spots of ceramide-1-phosphate was estimated with an image analyzer system (BAS III; Fuiji) and expressed as PSL arbitrary units (54), and ceramide levels were corrected for phospholipid phosphate as described elsewhere (57).

Statistical analysis. Statistical significance was evaluated by unpaired *t* tests and by analysis of variance as applicable; $P < 0.01$ was considered statistically significant.

Online supplemental material. Fig. S1 shows concentration of Triton X-100 for lipid raft separation. Fig. S2 shows early timecourse of caspase-8 activity, ceramide generation in lipid rafts, Fas redistribution into lipid rafts, and Fas multimer formation. Online supplemental material is available at http://www.jem.org/cgi/content/full/jem.20041685/DC1.

We thank Drs. H. Inoue and S. Goda of Osaka Dental University for technical assistance.

This work was supported by grants 13557160, 15024236, and 15390313 (to H. Umehara) from the Japanese Ministry of Education and Science and Culture, by the Uehara Memorial Foundation, and by grant P04244 (to Z.-X. Jin) from the Japan Society for the Promotion of Science.

The authors have no conflicting financial interests.

Submitted: 19 August 2004
Accepted: 2 May 2005

REFERENCES

1. Marsden, V.S., and A. Strasser. 2003. Control of apoptosis in the immune system: Bcl-2, BH-3 only proteins and more. *Annu. Rev. Immunol.* 21:71–105.
2. Scaffidi, C., S. Fulda, A. Srinivasan, C. Friesen, F. Li, K.J. Tomaselli, K.M. Debatin, P.H. Krammer, and M.E. Peter. 1998. Two CD95 (APO-1/Fas) signaling pathways. *EMBO J.* 17:1675–1687.
3. Wajant, H. 2002. The Fas signaling pathway: more than a paradigm. *Science.* 296:1635–1636.
4. Hengartner, M.O. 2000. The biochemistry of apoptosis. *Nature.* 407:770–776.
5. Simons, K., and E. Ikonen. 1997. Functional rafts in cell membranes. *Nature.* 387:569–572.
6. Brown, D.A., and E. London. 1998. Functions of lipid rafts in biological membranes. *Annu. Rev. Cell Dev. Biol.* 14:111–136.
7. Grassme, H., A. Jekle, A. Riehle, H. Schwarz, J. Berger, K. Sandhoff, R. Kolesnick, and E. Gulbins. 2001. CD95 signaling via ceramide-rich membrane rafts. *J. Biol. Chem.* 276:20589–20596.
8. Inoue, H., O. Yoneda, Y. Minami, Y. Tanaka, T. Okazaki, H. Imai, E. Bloom, N. Domae, and H. Umehara. 2002. Lipid rafts as the signaling scaffold for NK cell activation: tyrosine phosphorylation and association of LAT with PI 3-kinase and PLC-γ following CD2 stimulation. *Eur. J. Immunol.* 32:2188–2198.
9. Delmas, D., C. Rebe, S. Lacour, R. Filomenko, A. Athias, P. Gambert, M. Cherkaoui-Malki, B. Jannin, L. Dubrez-Daloz, N. Latruffe, and E. Solary. 2003. Resveratrol-induced apoptosis is associated with Fas redistribution in the rafts and the formation of a death-inducing signaling complex in colon cancer cells. *J. Biol. Chem.* 278:41482–41490.
10. Cremesti, A., F. Paris, H. Grassme, N. Holler, J. Tschopp, Z. Fuks, E. Gulbins, and R. Kolesnick. 2001. Ceramide enables Fas to cap and kill. *J. Biol. Chem.* 276:23954–23961.
11. Grassme, H., A. Cremesti, R. Kolesnick, and E. Gulbins. 2003. Ceramide-mediated clustering is required for CD95-DISC formation. *Oncogene.* 22:5457–5470.
12. Yamaoka, S., M. Miyaji, T. Kitano, H. Umehara, and T. Okazaki. 2004. Expression cloning of a human cDNA restoring sphingomyelin synthesis and cell growth in sphingomyelin synthase-deficient cells. *J. Biol. Chem.* 279:18688–18693.
13. Huitema, K., J.V.D. Dikkenberg, J.F. Brouwers, and J.C. Holthuis. 2004. Identification of a family of animal sphingomyelin synthases. *EMBO J.* 23:33–44.
14. Yamaji, A., Y. Sekizawa, K. Emoto, H. Sakuraba, K. Inoue, H. Kobayashi, and M. Umeda. 1998. Lysenin, a novel sphingomyelin-specific binding protein. *J. Biol. Chem.* 273:5300–5306.
15. Itoh, N., S. Yonehara, A. Ishii, M. Yonehara, S. Mizushima, M. Sameshima, A. Hase, Y. Seto, and S. Nagata. 1991. The polypeptide encoded by the cDNA for human cell surface antigen Fas can mediate apoptosis. *Cell.* 66:233–243.
16. Yamaji-Hasegawa, A., A. Makino, T. Baba, Y. Senoh, H. Kimura-Suda, S.B. Sato, N. Terada, S. Ohno, E. Kiyokawa, M. Umeda, and T. Kobayashi. 2003. Oligomerization and pore formation of a sphingomyelin-specific toxin, lysenin. *J. Biol. Chem.* 278:22762–22770.
17. Sato, S.B., K. Ishii, A. Makino, K. Iwabuchi, A. Yamaji-Hasegawa, Y. Senoh, I. Nagaosa, H. Sakuraba, and T. Kobayashi. 2004. Distribution and transport of cholesterol-rich membrane domains monitored by a membrane-impermeant fluorescent polyethylene glycol-derivatized cholesterol. *J. Biol. Chem.* 279:23790–23796.
18. Mundle, S.D., and A. Raza. 2002. Defining the dynamics of self-assembled Fas-receptor activation. *Trends Immunol.* 23:187–194.
19. Siegel, R.M., J.K. Frederiksen, D.A. Zacharias, F.K.M. Chan, M. Johnson, D. Lynch, R.Y. Tsien, and M. Lenardo. 2000. Fas preassociation required for apoptosis signaling and dominant inhibition by pathogenic mutations. *Science.* 288:2354–2357.
20. Chan, F.K.M., H.J. Chun, L. Zheng, R.M. Siegel, K.L. Bui, and M.J. Lenardo. 2000. A domain in TNF receptors that mediates ligand-independent receptor assembly and signaling. *Science.* 288:2351–2354.
21. Golstein, P. 2000. FasL binds preassembled Fas. *Science.* 288:2328–2329.
22. Kamitani, T., H.P. Nguyen, and E.T.H. Yeh. 1997. Activation-induced aggregation and processing of the human Fas antigen. *J. Biol. Chem.* 272:22307–22314.
23. Lee, Y.-J., and E. Shacter. 2001. Fas aggregation does not correlate with Fas-mediated apoptosis. *J. Immunol.* 167:82–89.
24. Dykstra, M., A. Cherukuri, H.W. Sohn, S.J. Tzeng, and S.K. Pierce. 2003. Location is everything: lipid rafts and immune cell signaling. *Annu. Rev. Immunol.* 21:457–481.
25. Muppidi, J., and R.M. Siegel. 2004. Ligand-independent redistribution of Fas (CD95) into lipid rafts mediates clonotypic death. *Nat. Immunol.* 5:182–189.
26. Kondo, T., K. Iwai, T. Kitano, M. Watanabe, Y. Taguchi, T. Yabu, H. Umehara, N. Domae, T. Uchiyama, and T. Okazaki. 2002. Control of ceramide-induced apoptosis by IGF-1: involvement of PI-3 kinase, caspase-3 and catalase. *Cell Death Differ.* 9:682–692.
27. Iwai, K., T. Kondo, M. Watanabe, T. Yabu, Y. Taguchi, H. Umehara, A. Takahashi, T. Uchiyama, and T. Okazaki. 2003. Ceramide increases oxidative damage due to inhibition of catalase by caspase-3-dependent proteolysis in HL-60 cell apoptosis. *J. Biol. Chem.* 278:9813–9822.
28. Watanabe, I., T. Kitano, T. Kondo, T. Yabu, Y. Taguchi, M. Tashima, H. Umehara, N. Domae, T. Uchiyama, and T. Okazaki. 2004. Increase of nuclear ceramide through caspase-3-dependent regulation of the "sphingomyelin (SM) cycle" in Fas-induced apoptosis. *Cancer Res.* 64:1000–1007.
29. Tepper, A.D., P. Ruurs, T. Wiedmer, P.J. Sims, J. Borst, and W.J. van Blitterswijk. 2000. Sphingomyelin hydrolysis to ceramide during the execution phase of apoptosis results from phospholipid scrambling and alters cell-surface morphology. *J. Cell Biol.* 150:155–164.

30. Hetz, C.A., M. Hunn, P. Rojas, V. Torres, L. Leyton, and A.F.G. Quest. 2002. Caspase-dependent initiation of apoptosis and necrosis by the Fas receptor in lymphoid cells: onset of necrosis is associated with delayed ceramide increase. *J. Cell Sci.* 115:4671–4683.
31. Blitterswijk, W.J.V., A.H. van der Luit, R.J. Veldman, and J. Borst. 2003. Ceramide: second messenger or modulator of membrane structure and dynamics? *Biochem. J.* 369:199–211.
32. Gulbins, E., and H. Grassme. 2002. Ceramide and cell death receptor clustering. *Biochim. Biophys. Acta.* 1585:139–145.
33. Kolesnick, R., and Z. Fuks. 2003. Radiation and ceramide-induced apoptosis. *Oncogene.* 22:5897–5906.
34. Pettus, B.J., C.E. Chalfant, and Y.A. Hannum. 2002. Ceramide in apoptosis: an overview and current perspective. *Biochim. Biophys. Acta.* 1585:114–125.
35. Sawai, H., T. Okazaki, Y. Takeda, M. Tashima, H. Sawada, M. Okuma, S. Kishi, H. Umehara, and N. Domae. 1997. Ceramide-induced translocation of protein kinase C-delta and -epsilon to the cytosol. *J. Biol. Chem.* 272:2452–2458.
36. Kondo, T., Y. Suzuki, T. Kitano, K. Iwai, M. Watanabe, H. Umehara, N. Daido, N. Domae, M. Tashima, T. Uchiyama, and T. Okazaki. 2002. Vesnarinone causes oxidative damage by inhibiting catalase function through ceramide action in myeloid cell apoptosis. *Mol. Pharmacol.* 61:620–627.
37. Uchida, Y., M. Itoh, Y. Taguchi, S. Yamaoka, M. Umeda, S. Ichikawa, Y. Hirabayashi, W.M. Holleran, and T. Okazaki. 2004. Ceramide reduction and transcriptional up-regulation of glucosylceramide synthase through Doxorubicin-activated Sp1 in drug-resistant HL-60/ADR cells. *Cancer Res.* 64:6271–6279.
38. Paris, F., H. Grassme, A. Cremesti, J. Zager, Y. Fong, A. Haimovitz-Friedman, Z. Fuks, E. Gulbins, and R. Kolesnick. 2001. Natural ceramide reverses Fas resistance of acid sphingomyelinase$^{-/-}$ hepatocytes. *J. Biol. Chem.* 276:8297–8305.
39. Schneider, P., N. Holler, J.-L. Bodmer, M. Hahne, K. Frei, A. Fontana, and J. Tschopp. 1998. Conversion of membrane-bound Fas (CD95) ligand to its soluble form is associated with down-regulation of its proapoptotic activity and loss of liver toxicity. *J. Exp. Med.* 187: 1205–1213.
40. Huang, D.C.S., M. Hahne, M. Schroeter, K. Frei, A. Fontana, A. Villunger, K. Newton, J. Tschopp, and A. Strasser. 1999. Activation of Fas by FasL induces apoptosis by a mechanism that cannot be blocked by Bcl-2 or Bcl-XL. *Proc. Natl. Acad. Sci. USA.* 96:14871–14876.
41. Papoff, G., P. Hausler, A. Eramo, M.G. Pagano, G.D. Leve, A. Signore, and G. Ruberti. 1999. Identification and characterization of a ligand-independent oligomerization domain in the extracellular region of the CD95 death receptor. *J. Biol. Chem.* 274:38241–38250.
42. Gulbins, E., and R. Kolesnick. 2003. Raft ceramide in molecular medicine. *Oncogene.* 22:7070–7077.
43. Cherukuri, A., M. Dykstra, and S.K. Pierce. 2001. Floating the raft hypothesis: Lipid rafts play a role in immune cell activation. *Immunity.* 14: 657–660.
44. Bromley, S.K., W.R. Burack, K.G. Johnson, K. Somersalo, T.N. Sims, C. Sumen, M.M. Davis, A.S. Shaw, P.M. Allen, and M.L. Dustin. 2001. The immunological synapse. *Annu. Rev. Immunol.* 19:375–396.
45. Davis, D.M. 2002. Assembly of the immunological synapse for T cell and NK cells. *Trends Immunol.* 23:356–363.
46. London, M., and L. Erwin. 2004. Ceramide selectively displaces cholesterol from ordered lipid domain (Rafts). *J. Biol. Chem.* 279:9997–10004.
47. Veiga, M.P., J.L.R. Arrondo, F.M. Goni, and A. Alonso. 1999. Ceramides in phospholipid membranes: effects on bilayer stability and transition to nonlamellar phases. *Biophys. J.* 76:342–350.
48. Holopainen, J.M., M. Subramanian, and P.K. Kinnunen. 1998. Sphingomyelinase induces lipid microdomain formation in a fluid phosphatidylcholine/sphingomyelin membrane. *Biochemistry.* 37:17562–17570.
49. Grassme, H., V. Jendrossek, A. Riehle, G. von Kurthy, J. Berger, H. Schwarz, M. Weller, R. Kolesnick, and E. Gulbins. 2003. Host defence against *Pseudomonas aeruginosa* requires ceramide-rich membrane rafts. *Nat. Med.* 9:322–330.
50. Okazaki, T., R.M. Bell, and Y.A. Hannun. 1989. Sphingomyelin turnover induced by vitamin D3 in HL-60 cells. *J. Biol. Chem.* 264: 19076–19080.
51. Liu, P., and R.G. Anderson. 1995. Compartmentalized production of ceramide at the cell surface. *J. Biol. Chem.* 270:27179–27185.
52. Algeciras-Schimnich, A., L. Shen, B.C. Barnhart, A.E. Murmann, J.K. Burkhardt, and M.E. Peter. 2002. Molecular ordering of the initial signaling events of CD95. *Mol. Cell. Biol.* 22:207–220.
53. Bligh, E., and W. Dyer. 1959. A rapid method of total lipid extraction and purification. *Can. J. Biochem. Physiol.* 37:911–917.
54. Umehara, H., J.-Y. Huang, T. Kono, F.H. Tabassam, T. Okazaki, E.T. Bloom, and N. Domae. 1997. Involvement of protein tyrosine kinase $p72^{syk}$ and phosphatidylinositol 3-kinase in CD2-mediated granular exocytosis in natural killer cell line. *J. Immunol.* 159:1200–1207.
55. Umehara, H., J.-Y. Huang, T. Kono, F.H. Tabassam, T. Okazaki, S. Gouda, Y. Nagano, E.T. Bloom, and N. Domae. 1998. Co-stimulation of T cells with CD2 augments TCR-CD3-mediated activation of protein tyrosine kinase $p72^{syk}$, resulting in increased tyrosine phosphorylation of adapter proteins, Shc and Cbl. *Int. Immunol.* 10:833–845.
56. Rodgers, W., and J.K. Rose. 1996. Exclusion of CD45 inhibits activity of $p56^{lck}$ associated with glycolipid-enriched membrane domains. *J. Cell Biol.* 135:1515–1523.
57. Okazaki, T., A. Bielawska, R.M. Bell, and Y.A. Hannun. 1990. Role of ceramide as a lipid mediator of 1 alpha, 25-dehydroxyvitamin D3-induced HL-60 cell differentiation. *J. Biol. Chem.* 265:15823–15831.

Mod Rheumatol (2008) 18:15–22
DOI 10.1007/s10165-007-0015-y

ORIGINAL ARTICLE

Interleukin-17 gene expression in patients with rheumatoid arthritis

Mika Kohno · Akito Tsutsumi · Hiroto Matsui · Makoto Sugihara · Takeshi Suzuki · Mizuko Mamura · Daisuke Goto · Isao Matsumoto · Satoshi Ito · Toru Suguro · Takayuki Sumida

Received: 14 August 2007 / Accepted: 28 September 2007 / Published online: 20 December 2007

Abstract Interleukin-17 is a proinflammatory cytokine. Recent animal studies have shown that IL-17 plays a role in the initiation and progression of arthritis. However, whether IL-17 has a prominent role in human rheumatoid arthritis (RA) or not remains unclear. Here we investigated the role of IL-17 in patients with RA. cDNA was prepared from knee joint synovial tissues of RA ($n = 11$) and osteoarthritic (OA, $n = 10$) patients and PBMC of RA ($n = 52$) and healthy subjects ($n = 34$). IL-17 gene expression level was measured by real-time PCR, and was compared with various clinical parameters. IL-17 gene expression in synovial tissues of RA was similar to that in OA. IL-17 gene expression level in PBMC of RA patients was significantly higher than in the control. The response (changes in DAS) to two-week treatment with anti-TNF-α blockers (infliximab or etanercept) did not correlate with changes in IL-17 gene expression levels. The IL-17/TNF-α gene expression ratio at baseline (before treatment) tended to be lower in responders to the treatment. Expression of IL-17 gene in PBMC may be associated with the inflammatory process of RA. IL-17/TNF-α expression ratio is a potentially suitable marker of response to anti-TNF-α therapy.

M. Kohno · A. Tsutsumi · H. Matsui · M. Sugihara · T. Suzuki · M. Mamura · D. Goto · I. Matsumoto · S. Ito · T. Sumida (✉)
Division of Clinical Immunology, Major of Advanced Biomedical Applications, Graduate School Comprehensive Human Science, University of Tsukuba, 1-1-1 Tennnodai, Tsukuba 305-8575, Japan
e-mail: tsumida@md.tsukuba.ac.jp

T. Suguro
Department of Orthopaedic Surgery, School of Medicine, Toho University, Tokyo, Japan

Keywords Etanercept · Infliximab · Interleukin-17 (IL-17) · Rheumatoid arthritis · Tumor necrosis factor-α (TNF-α)

Introduction

Rheumatoid arthritis (RA) is characterized by chronic synovial inflammation, cartilage degradation and bone erosion in multiple joints, which ultimately lead to joint destruction and disability. Inflammatory cytokines such as tumor necrosis factor α (TNF-α), interleukin-1 (IL-1) and IL-6 are involved in the pathogenesis of RA [1–3], and the beneficial effects of antagonists to these cytokines have been reported [4–6]. However, not all patients respond to these agents, suggesting that other pro-inflammatory cytokines, e.g., IL-17, may be important in the pathogenesis of RA.

IL-17 is a proinflammatory cytokine produced by activated and memory $CD4^+$ $CD45RO^+$ T cells [7–8], and is a potent inducer of other cytokines, such as TNF-α, IL-1β, IL-6, IL-8, and granulocyte colony stimulating factor (G-CSF) in a variety of epithelial, endothelial, and fibroblastic cell types [9]. In experimental arthritis, IL-17 was found to be important in both the early initiation phase and late progression phase, especially in arthritis models driven mainly by T cells, such as the IL-1 $Ra^{-/-}$ mouse model and streptococcal cell wall-induced arthritis [10–15].

Several studies have suggested that IL-17 plays a role in the pathogenesis of RA. Chabaud et al. [16] reported that the proportion of synovial membrane cultures that produced IL-17 was higher in those from RA patients than those from OA patients or healthy controls. In addition, previous studies indicated the presence of elevated IL-17 levels in the synovial fluid of patients with sRA [17, 18].

Although these observations imply that IL-17 is involved in the pathogenesis of human RA, there is no solid information on whether IL-17 actually plays a role in RA pathogenesis.

With regard to TNF-α, previous studies reported that IL-17 contributes to the arthritic process not only by inducing the production of TNF-α, but also acting in synergy with or independently of TNF-α [8, 19–23]. Although it is unknown whether these observations are relevant in human RA, we hypothesized that IL-17 gene expression level in PBMC might be enhanced independent of that of TNF-α in some patients with RA, and that these patients may comprise a subpopulation of RA refractory to anti-TNF-α therapy.

The aims of the present study were to clarify the role of IL-17 in disease activity and progression of human RA and to explore the possibility of IL-17 as a target for the treatment for RA. For this purpose, we measured the gene expression of IL-17 in peripheral blood mononuclear cells (PBMC) and synovial tissues from RA patients. We correlated the findings of PBMC samples with various clinical parameters, TNF-α gene expression and the efficacy of infliximab or etanercept.

Methods

Patients

Peripheral blood was taken from 52 patients who fulfilled the 1987 American Rheumatism Association criteria for the classification of RA [24]. The patient group comprised 19 males and 33 females (age, 25–84 years, mean ± SD: 54.0 ± 13.0 years). The fifty-two RA patients included 25 infliximab- and 11 etanercept-treated patients who attended our unit between 29 September 2003 and 22 August 2006, and, as a control group, 16 RA patients who visited our unit between October 11 and October 25 2006. Clinical data such as white blood cell count (WBC), erythrocyte sediment rate (ESR), c-reactive protein (CRP) and matrix metalloproteinase 3 (MMP-3) was obtained at the time of blood sampling. We also included a group of control healthy donors (13 men and 21 women, age 30.0 ± 5.0 years). Synovial tissues were obtained at the time of total knee replacement performed from April 2001 to June 2002 on 11 RA patients (one male and ten females, age 56.8 ± 8.7 years) and ten osteoarthritis (OA) patients (ten females, age 73.4 ± 2.7 years). No patient underwent both blood and synovial tissue sampling. Patient demographics are listed in Table 1. Written informed consent was obtained from all subjects, and the study was approved by the appropriate ethics committee.

Treatment with infliximab or etanercept and assessment of efficacy

Twenty-five RA patients were treated with 3 mg/kg of infliximab at weeks 0, 2, 6, and 14, and every eight weeks thereafter. Another RA group consisting of 11 patients were treated with etanercept (25 mg injection twice weekly). Drug efficacy was evaluated by comparing the differences in European League Against Rheumatism improvement criteria [Disease Activity Score (DAS)] at week 0 (before treatment) and at 2 weeks.

Synovial and blood samples for cDNA synthesis

Part of each synovial tissue was cut into small pieces and rinsed with phosphate-buffered saline (PBS). Complementary DNA (cDNA) was prepared from synovial tissues

Table 1 Demographics of the subjects included in the study

PBMC	Mean ± SD	Range	Synovium	Mean ± SD	Range
RA patients			RA patients		
Age (years)	54.0 ± 13.0	(25–84)	Age (years)	56.8 ± 8.7	(37–70)
Males	19		Males	1	
Females	33		Females	10	
C-reactive protein (mg/dl)	2.15 ± 1.63	(0.25–8.95)	C-reactive protein (mg/dl)	1.65 ± 2.64	(0.07–7.17)
ESR (mm/h)	48.5 ± 21.1	(12–104)	ESR (mm/h)	33.4 ± 25.1	(10–95)
Rheumatoid factor (IU/ml)	245 ± 231	(5–1790)	Rheumatoid factor (IU/ml)	161 ± 199	(4–715)
Healthy controls			OA patients		
Age (years)	30.0 ± 5.0	(22–50)	Age (years)	73.4 ± 2.7	(69–78)
Males	13		Males	0	
Females	21		Females	10	

ESR erythrocyte sedimentation rate

using Revertaid first strand cDNA synthesis kit (Fermentas, Hanover, MD, USA), following the instructions provided by the manufacturer.

Peripheral blood mononuclear cells (PBMC) were isolated from heparinized peripheral blood obtained from normal subjects and RA patients using Ficoll-Paque PLUS (Amersham Biosciences, Uppsala, Sweden) following the protocol recommended by the manufacturer. Cells were spun down to pellets and total RNA was extracted from the cell pellets using Isogen (Nippongene, Tokyo, Japan). The cDNAs were synthesized using a Revertaid first strand cDNA synthesis kit (Fermentas), following the instructions provided by the manufacturer. These cDNA samples underwent gene expression analyses.

Quantification of gene expression by real-time polymerase chain reaction

The cDNA samples were amplified with specific primers and fluorescence-labeled probes for the target genes. Specific primers and probes for IL-17, IL-6, TNF-α and glyceraldehyde-2-phosphate dehydrogenase (GAPDH) were purchased from Applied Biosystems Japan (Tokyo). The amplified product genes were monitored on an ABI 7700 sequence detector (Applied Biosystems Japan). The qPCR master mix was also purchased from Applied Biosystems Japan. The final concentrations of the primers were 200 nM for each of the 5′ and 3′ primers, and the final probe concentration was 100 nM. The thermal cycler conditions used were 50 °C for 2 min, 95 °C for 10 min, then 50 cycles of 95 °C for 15 s and 60 °C for 1 min. Serial dilutions of a standard sample were included in every assay, and standard curves for the genes of interest and GAPDH genes were generated. All measurements were performed in triplicate. The level of gene expression was calculated from the standard curve, and expressed relative to GAPDH gene expression.

Statistical analysis

All data were expressed as mean ± standard deviation (SD). The Mann–Whitney U test was used to compare the expression levels of genes between RA patients and healthy controls. Spearman's correlation coefficient by rank test was calculated to assess the correlations between the expression levels of IL-17 and TNF-α genes, as was the correlation between IL-17/TNF-α gene expression ratio and changes in DAS after two weeks of therapy with etanercept or infliximab relative to baseline (before treatment, i.e., DAS 0–2 weeks). Paired Wilcoxon's rank test was used to compare the gene expression levels between week 0 and week 2. A P value of less than 0.05 was considered significant.

Results

Expression levels of IL-17 genes in synovial tissues

We anticipated that the expression of IL-17 would be enhanced in RA patients at the site of inflammation, namely the synovial tissue. However, the expression of IL-17 gene in synovial tissues of RA patients, as measured by real-time PCR, was not significantly different from that of the OA patients (Fig. 1).

Expression levels of IL-17 genes in PBMC

We next asked whether the expression level of IL-17 gene is upregulated in PBMC of RA patients. Expression of the IL-17 gene in PBMC from RA patients was significantly higher than that of the control (RA: 0.0437 ± 0.1112, control: 0.0134 ± 0.0033, P = 0.011, Fig. 2).

Relationship between IL-17 and IL-6 or TNF-α gene expression in RA patients

We wished to determine whether the expression of IL-17 gene in patients with RA is significantly associated with

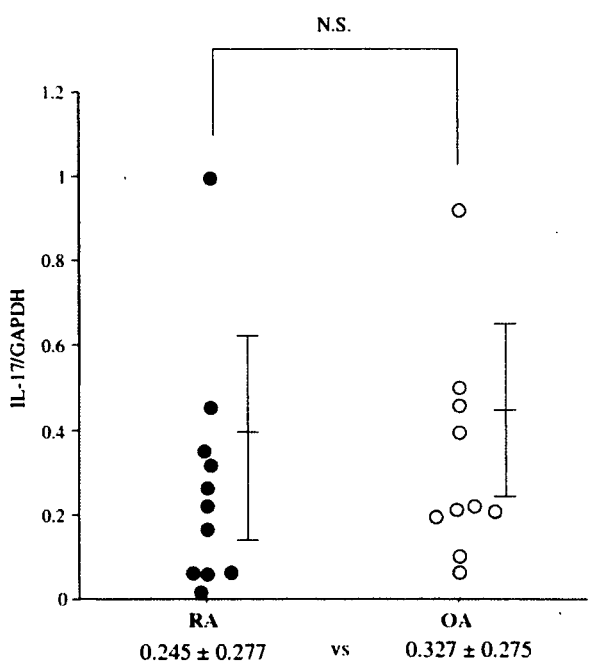

Fig. 1 Expression levels of IL-17 gene in the synovium tissues of patients with RA (*closed circles*, n = 11) and osteoarthritis (OA, *open circles*, n = 10). Data are mean ± SD. The P value was calculated by the Mann–Whitney U test

expressions of other inflammatory cytokines such as TNF-α and IL-6. No significant relationship between expression of the IL-17 gene and that of IL-6 or TNF-α was observed (Fig. 3a, b). In addition, there was no significant relationship between the expression level of IL-6 and that of TNF-α (Fig. 3c). Furthermore, the expression levels of IL-17 in PBMC of RA patients did not correlate significantly with WBC count, serum CRP, ESR or serum MMP-3 (data not shown).

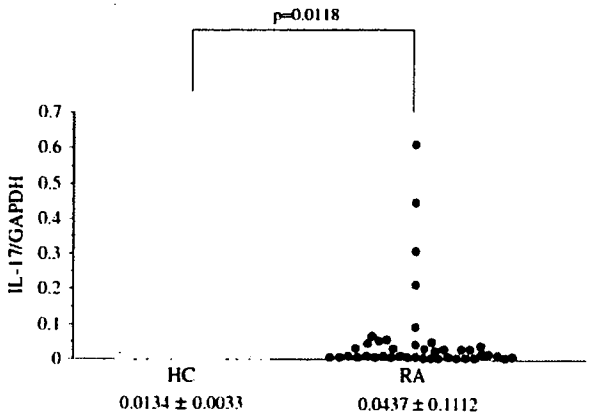

Fig. 2 Expression levels of IL-17 gene in peripheral blood mononuclear cells from patients with RA (*closed circles*, $n = 52$) and from healthy controls (HC, *open circles*, $n = 34$). Data are mean ± SD. The P values were calculated by the Mann–Whitney U test

Effects of infliximab and etanercept therapy on IL-17 gene expression in PBMC

We compared the gene expression levels of IL-17 in PBMC samples at baseline, and two weeks after the first infusion or injection of biologics that target TNF-α. In patients who received infliximab, no significant differences were observed between baseline and week 2 samples (week 0: 0.089 ± 0.157, week 2: 0.044 ± 0.056, Fig. 4a). On the other hand, etanercept significantly increased IL-17 gene expression at two weeks after initiation of therapy (week 0: 0.041 ± 0.132, week 2: 0.134 ± 0.274, $P = 0.028$, Fig. 4 b). There were no relationships between changes in IL-17 gene expression levels and efficacy (changes in DAS) of infliximab and etanercept.

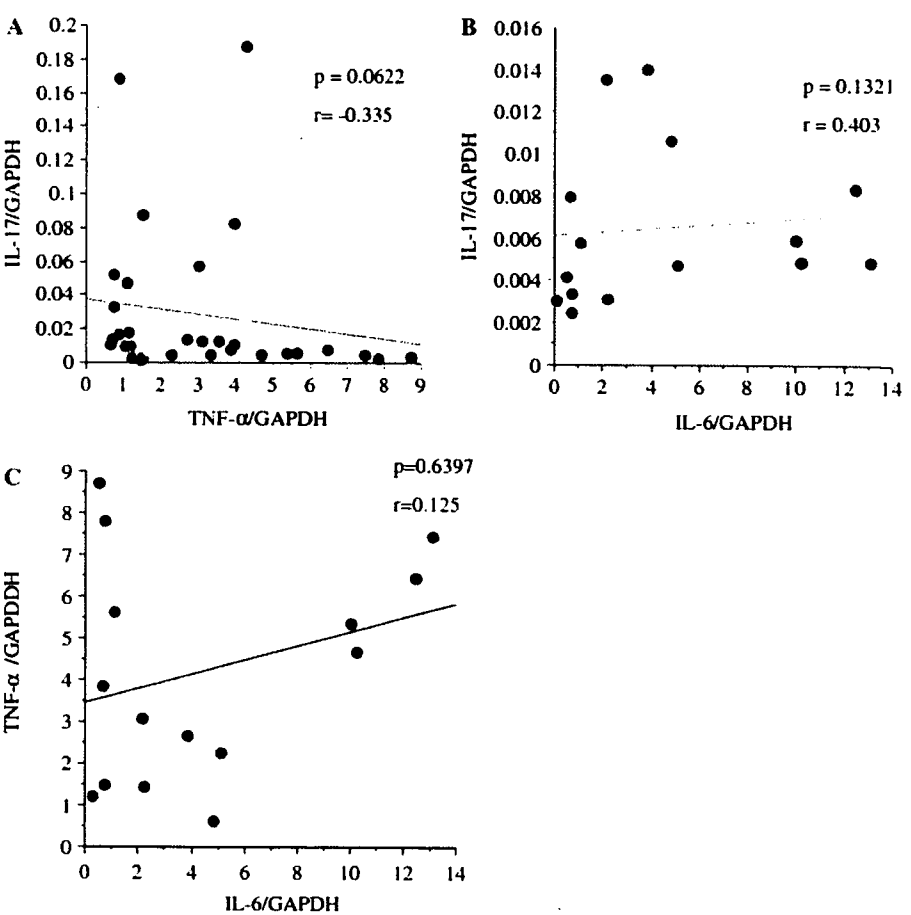

Fig. 3 Relationships between expression levels of IL-17, TNF-α and IL-6 genes in peripheral blood mononuclear cells from rheumatoid arthritis (RA) patients. a Relationship between expression levels of IL-17 and TNF-α in PBMC from RA ($n = 31$). b Relationship between expression levels of IL-17 and IL-6 in PBMC from RA ($n = 15$). c Relationship between expression levels of TNF-α and IL-6 in PBMC from RA ($n = 15$) r = correlation coefficient. The P values were calculated by Spearman's correlation coefficient by rank test

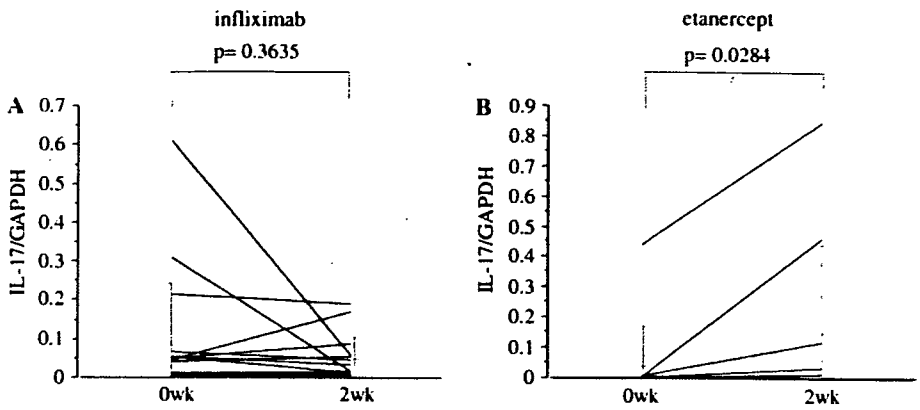

Fig. 4 IL-17 gene expression levels in peripheral blood mononuclear cells at baseline and two weeks after the first infusion of infliximab (n = 17) (a), and after the first injection of etanercept (n = 11) (b). Data are mean ± SD. The P values were calculated by Wilcoxon's rank sum test

Relationships between IL-17 and TNF-α gene expression and efficacy of anti-TNF-α therapy

We next examined whether patients with a high expression level of IL-17 gene relative to that of the TNF-α gene were more refractory to anti-TNF-α therapy. For this purpose, we calculated the IL-17/TNF-α gene expression ratio in PBMC of RA patients prior to anti-TNF-α therapy and correlated it with changes in DAS from pre- to two-week post-therapy (DAS0-2 week). The results showed that the IL-17/TNF-α gene expression ratio prior to treatment tended to be lower in patients who responded to anti-TNFα therapy, although the relationship was not statistically significant (Fig. 5).

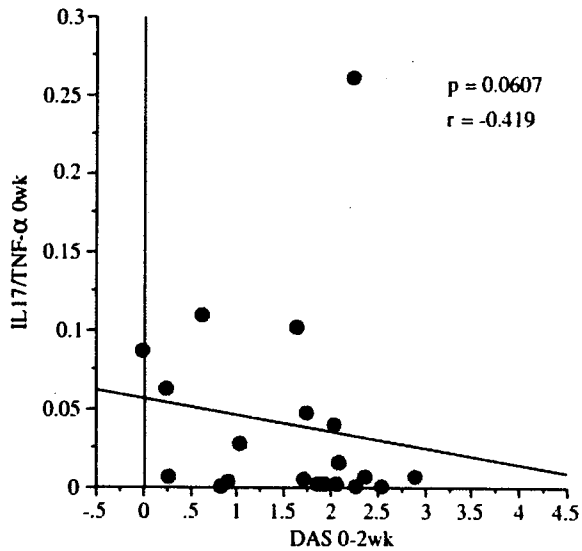

Fig. 5 Relationship between IL-17/TNF-α ratio in peripheral blood mononuclear cells and response to anti-TNF-α therapy. Number of patients = 20, r = correlation coefficient. The P values were calculated by Spearman's correlation coefficient by the rank test

Discussion

The active involvement of IL-17 in both the initiation stage and the progression stage of murine experimental arthritis has been demonstrated and IL-17 is considered a key cytokine in the pathogenesis of arthritis in such experimental models [10–13]. A few studies suggest that IL-17 may have a role in the pathogenesis of human RA as well [16–18].

Based on the above background, we measured IL-17 gene expression in synovial tissues and PBMC of RA patients, and compared them with those in control samples. We first compared the expression of IL-17 gene in synovial tissues from RA patients with that in OA patients. Unexpectedly, the IL-17 gene expression level in synovial tissues of OA patients was comparable to that in RA patients. This result is in contrast to that described by Chabaud et al. [16], where expression of IL-17 gene was higher in RA synovium than in OA synovium. Differences in patient demographics and sample size may partly account for this discrepancy. While OA is not generally considered an inflammatory disorder, it is reported that IL-17 upregulates the release of IL-8 and GRO-α in synovial fibroblasts and chondrocytes isolated from patients from OA, suggesting that IL-17 does play a role in the joint destruction process of OA [25]. In this study, we were unable to obtain synovial tissues from healthy individuals, which would have been a better control for this study. In contrast to our study, Kotake et al. [17] reported the presence of high IL-17 protein levels in synovial fluids of patients with RA, but not those with OA. The reason for this discrepancy is unclear, but it is possible that differences in post-transcription regulation of IL-17 production between RA and OA partly contributes to the difference in protein levels in the synovial fluid.

We next examined whether IL-17 gene expression in PBMC is elevated in patients with RA. As expected, the expression of IL-17 gene was significantly higher in PBMC of RA patients than in those of healthy controls. This result

implies that IL-17 does have a role in the inflammatory process of RA, at least in some patients. We did not measure expression of the IL-17 gene in PBMC from OA patients. Comparison of IL-17 gene expression in synovial tissues and PBMC taken simultaneously in both RA patients and OA patients could be informative. Expression of the IL-17 gene in PMBC of RA patients differed greatly among individuals, suggesting that such expression is important in some patients at some points during the course of the disease. Future studies with serial samples from RA patients would be informative. In this regard, IL-17 protein levels were undetectable in serum samples of 15 RA and 15 healthy controls (<15.6 pg/ml) by enzyme immunoassay (data not shown). Thus, we were unable to determine whether IL-17 gene expression levels in PBMC reflect the levels of serum IL-17 protein.

Interleukin-17 is known to enhance the pro-inflammatory effects of TNF-α in vitro and to act in synergy with TNF-α in the progression of arthritis in experimental arthritis mouse models [8, 19, 20, 21]. IL-17 is reported to depend strongly on TNF-α in induction of arthritis under naïve conditions in another experimental arthritis model [15]. However, it was recently reported that IL-17 could induce arthritis in the absence of TNFα in an experimental arthritis model [22]. Therefore, we considered it possible that (1) the expression of IL-17 gene in PBMC may be related to that of TNF-α, or (2) some RA patients show enhanced IL-17 gene expression level in PBMC regardless of the TNFα gene expression level, and comprise a subpopulation of anti-TNF-α refractory patients. We found a tendency towards a negative relationship between the expression of IL-17 gene and that of TNF-α gene in PBMC of RA patients, although the relationship was not significant. In addition, we found no significant relationship between IL-17 gene expression in PBMC and various parameters of inflammation, including ESR and serum CRP. These results imply that, in RA, which is a multifactorial and heterogeneous disease, gene expressions of TNF-α and IL-17 in PBMC are not directly associated with each other, and the expression of IL-17 in PBMC does not have an overwhelming influence on the inflammatory status.

Interleukin-6 is also a pro-inflammatory cytokine known to play an important role in the pathogenesis of RA [26, 27], and also to regulate the differentiation of Th17 T cells. Previous studies indicated that IL-6$^{-/-}$CD4+ T cells from draining lymph nodes produced less IL-17 than cells from wild-type mice, and that IL-6-deficient SKG mice were completely devoid of IL-17^{+}CD4+ T cells [28–30]. Conversely, IL-17 induced secretion of IL-6 from cultured fibroblasts [7, 8]. Based on this background, we compared the expression of IL-17 and IL-6 genes in PBMC of RA patients. In contrast to the relationship between IL-17 gene expression and TNF-α gene expression, a tendency towards a positive relationship was observed, albeit statistically insignificant.

It has been reported that IL-23 is important in the survival and expansion of IL-17- and IL-6-producing Th17 T cells and the development of collagen-induced arthritis in mice [30–33]. A recent study reported that self-reactive T cells produced by genetic alteration of thymic T cell selection spontaneously differentiate into Th17 T cells, and that these T cells stimulate antigen presenting cells (APC) to secrete IL-6 [29]. APC-derived IL-6 and T-cell derived IL-6 drive naïve T cells to differentiate into arthritogenic Th17 T cells [34]. Our observation may reflect the fact that Th17 T cells have an important role in the pathogenesis of human RA.

The efficacy of anti-TNF-α therapy in RA is well established [35]. However, non-responders hardly show any improvement in symptoms even after continuous injection or infusion of TNF-α antagonists. These observations imply that some cytokines other than TNF-α can act independently of TNF-α in the pathogenesis of RA. If IL-17 is one of these cytokines, IL-17 may become an appropriate target for treatment of RA patients refractory to TNF-α antagonists. To gain an insight into this question, we first addressed how TNF-α blockage affected the expression of IL-17 gene in PBMC of patients with RA by comparing IL-17 gene expression before and two weeks after the first infliximab or etanercept injection. Infliximab did not significantly affect IL-17 expression but etanercept significantly increased the expression in PBMC after two weeks of therapy. The reason for this difference is not clear at present. However, etanercept is known to be a decoy receptor and inhibitor of the action of soluble TNF-α, while infliximab is an antibody against TNF-α and is reported to induce negative signals through membrane TNF-α [36]. This may partly account for the observed differences in the action of these two agents. At present, we could not find any significant relationship between the efficacy of TNF-α blockade therapy and fluctuation of IL-17 gene expression in PBMC. A study in a larger number of patients is warranted to examine this issue.

We also calculated the IL-17/TNF-α ratio in PBMC of RA patients prior to initiation of therapy using TNF-α blocking agents, and examined the changes in the ratio after such treatment. While there was no relationship between DAS 0–2 week and IL-17 or TNF-α gene expression, the IL-17/TNF-α ratio tended to be lower in responders. These results suggest that RA patients with low IL-17 gene expression and high TNF-α gene expression in PBMC before treatment are more likely to respond to anti-TNF-α therapy. Currently there are no tools available to distinguish between responders and non-responders before TNF-α blockade therapy. IL-17/TNF-α expression ratio in

PBMC may be a suitable predictor of the response to treatment with TNF-α blockers.

In conclusion, we have demonstrated that IL-17 gene expression in PBMC of RA patients is higher than those in controls. We speculate that IL-17 might play an important role in the pathogenesis of RA, and that IL-17/TNF-α gene expression ratio in PBMC prior to infliximab or etanercept therapy may predict the response to treatment. Further studies are necessary to clarify the molecular basis of IL-17 action in the pathogenesis of RA and whether IL-17 is a suitable target for the treatment of RA.

References

1. Amer EC, Pratta MA. Independent effects of interleukin-1 on proteoglycan breakdown, proteoglycan synthesis, and prostaglandin E_2 release from cartilage in organ culture. Arthritis Rheum 1989;32:288–97.
2. Arend WP, Dayer J-M. Inhibition of the production and effects of interleukin-1 and tumor necrosis factor α in rheumatoid arthritis. Arthritis Rheum 1995;38:151–60.
3. Van de Loo FAJ, Joosten LAB, van Lent PLEM, Arntz OJ, van den Berg WB. Role of interleukin-1, tumor necrosis factor α, and interleukin-6 in cartilage proteoglycan metabolism and destruction: effect of in situ blocking in murine antigen- and zymosan-induced arthritis. Arthritis Rheum 1995;38:164–72.
4. Shanahan JC, St Clair W. Tumor necrosis factor alpha blockade: a novel therapy for rheumatic disease. Clin Immunol 2002;103:231–42.
5. Nishimoto N, Yoshizaki K, Miyasaka N, Yamamoto K, Kawai S, Takeuchi T, et al. Treatment of rheumatoid arthritis with humanized anti-interleukin-6 receptor antibody: a multicenter, double-blind, placebo-controlled trial. Arthritis Rheum 2004;50:1761–9.
6. Dayer JM, Feige U, Edwards CK 3rd, Burger D. Anti-interleukin-1 therapy in rheumatic diseases. Curr Opin Rheumatol 2001;13:170–6.
7. Yao Z, Painter SL, Fanslow WC, Ulrich D, Macduff BM, Spriggs MK, et al. Human IL-17: a novel cytokine derived from T cells. J Immunol 1995;155:5483–6.
8. Fossiez F, Djossou O, Chomarat P, Flores-Romo L, Ait-Yahia S, Maat C, et al. T cell interleukin-17 induces stromal cells to produce proinflammatory and hematopoietic cytokines. J Exp Med 1996;183:2593–603.
9. Aggarwal S, Gurney AL. IL-17: prototype member of an emerging cytokine family. J Leukoc Biol 2002;71:1.
10. Nakae S, Nambu A, Sudo K, Iwakura Y. Suppression of immune induction of collagen-induced arthritis in IL-17-deficient mice. J Immunol 2003;171:6173–7.
11. Nakae S, Saijo S, Horai R, Sudo K, Mori S, Iwakura Y. IL-17 production from activated T cells is required for the spontaneous development of destructive arthritis in mice deficient in IL-1 receptor antagonist. Proc Natl Acad Sci USA 2003;100:5986–90.
12. Lubberts E, Joosten LA, Oppers B, van den Bersselaar L, Coenen-de Roo CJ, Kolls JK, et al. IL-1-independent role of IL-17 in synovial inflammation and joint destruction during collagen-induced arthritis. J Immunol 2001;167:1004–13.
13. Lubberts E, Koenders MI, Oppers-Walgreen B, van den Bersselaar L, Coenen-de Roo CJ, Joosten LA, et al. Treatment with a neutralizing anti-murine interleukin-17 antibody after the onset of collagen-induced arthritis reduces joint inflammation, cartilage destruction, and bone erosion. Arthritis Rheum 2004;50:650–9.
14. Koenders MI, Lubberts E, Oppers-Walgreen B, van den Bersselaar L, Helsen MM, Di Padova FE, et al. Blocking of interleukin-17 during reactivation of experimental arthritis prevents joint inflammation and bone erosion by decreasing RANKL and interleukin-1. Am J Pathol 2005;167:141–9.
15. Koenders MI, Kolls JK, Oppers-Walgreen B, van den Bersselaar L, Joosten LA, Schurr JR, et al. Interleukin-17 receptor deficiency results in impaired synovial expression of interleukin-1 and matrix metalloproteinases 3, 9, and 13 and prevents cartilage destruction during chronic reactivated streptococcal cell wall-induced arthritis. Arthritis Rheum 2005;52:3239–47.
16. Chabaud M, Durand JM, Miossec P. Human interleukin-17: a T cell-derived proinflammatory cytokine produced by the rheumatoid synovium. Arthritis Rheum 1999;42:963–70.
17. Kotake S, Udagawa N, Takahashi N, Matsuzaki K, Itoh K, Ishiyama S, et al. IL-17 in synovial fluids from patients with rheumatoid arthritis is a potent stimulator of osteoclastogenesis. J Clin Invest 1999;103:1345–52.
18. Ziolkowska M, Koc A, Maslinski W. High levels of IL-17 in rheumatoid arthritis patients: IL-15 triggers in vitro IL-17 production via cyclosporin A-sensitive mechanism. J Immunol 2000;164:2832–8.
19. Chen YF, Jobanputra P, Barton P, Jowett S, Bryan S, Clark W et al. A systematic review of the effectiveness of adalimubub, etanercept and infliximab for the treatment of rheumatoid arthritis in adults and an economic exaluation of their cost-effectiveness. Health Technol Assess 2006;10:1–229.
20. Katz Y, Nadiv O, Beer Y. Interleukin-17 enhances tumor necrosis factor-α induced synthesis of interleukins 1,6, and 8 in skin and synovial fibroblasts: a possible role as a "fine-tuning cytokine" in inflammation processes. Arthritis Rheum 2001;44:2176–84.
21. LeGrand A, Fermor B, Fink C, Pisetsky DS, Weinberg JB, Vail TP, et al. Interleukin-1, tumor necrosis factor alpha, and interleukin-17 synergistically up-regulate nitric oxide and prostaglandin E2 production in explants of human osteoarthritic knee menisci. Arthritis Rheum 2001;44:2078–83.
22. Koenders MI, Lubberts E, van de Loo FA, Oppers-Walgreen B, van den Bersselaar L, Helsen MM, et al. Interleukin-17 acts independently of TNF-alpha under arthritic conditions. J Immunol 2006;176:6262–9.
23. Koenders MI, Joosten LA, van den Berg WB Potential new targets in arthritis therapy: interleukin (IL)-17 and its relation to tumour necrosis factor and IL-1 in experimental arthritis. Ann Rheum Dis 2006;65:29–33.
24. Arnett FC, Edworthy SM, Bloch DA, McShane DJ, Fries JF, Cooper NS, et al. The American Rheumatism Association 1987 revised criteria for the classification of rheumatoid arthritis. Arthritis Rheum 1988;31:315–24.
25. Honorati MC, Bovara M, Facchini A. Contribution of interleukin 17 to human cartilage degradation and synovial inflammation in osteoarthritis. Osteoarthritis Cartilage 2002;10:799–807.
26. Wong PK, Quinn JM, Sims NA, van Nieuwenhuijze A, Campbell IK, Wicks IP, et al. Interleukin-6 modulates production of T lymphocyte-derived cytokines in antigen-induced arthritis and drives inflammation-induced osteoclastogenesis. Arthritis Rheum 2006;54:158–68.
27. Nishimoto N. Clinical benefits of anti-human IL-6 receptor antibody therapy. Clin Calcium 2007;17:562–8.
28. Mangan PR, Harrington LE, O'Quinn DB, Helms WS, Bullard DC, Elson CO, et al. Transforming growth factor-beta induces development of the T(H)17 lineage. Nature 2006;441:231–4.
29. Hirota K, Hashimoto M, Yoshitomi H, Tanaka S, Nomura T, Yamaguchi T, et al. T cell self-reactivity forms a cytokine milieu for spontaneous development of IL-17+ Th cells that cause autoimmune arthritis. J Exp Med 2007;204:41–7.

30. Bettelli E, Carrier Y, Gao W, Korn T, Strom TB, Oukka M, et al. Reciprocal developmental pathways for the generation of pathogenic effector TH17 and regulatory T cells. Nature 2006;441:235–8.
31. Murphy CA, Langrish CL, Chen Y, Blumenschein W, McClanahan T, Kastelein RA, et al. Divergent pro- and antiinflammatory roles for IL-23 and IL-12 in joint autoimmune inflammation. J Exp Med 2003;198:1951–7.
32. Veldhoen M, Hocking RJ, Atkins CJ, Locksley RM, Stockinger B. TGF beta in the context of an inflammatory cytokine milieu supports de novo differentiation of IL-17 producing T cells. Immunity 2006;24:179–89.
33. Bettelli E, Oukka M, Kuchroo VK. T(H)-17 cells in the circle of immunity and autoimmunity. Nat Immunol 2007;8:345–50.
34. Hirota K, Hashimoto M, Yoshitomi H, Tanaka S, Nomura T, Yamaguchi T, et al. T cell self-reactivity forms a cytokine milieu for spontaneous development of IL-17+ Th cells that cause autoimmune arthritis. J Exp Med 2007;204:41–7.
35. Gaffo A, Saag KG, Curtis JR. Treatment of rheumatoid arthritis. Am J Health Syst Pharm 2006;63:2451–65.
36. Mitoma H, Horiuchi T, Hatta N, Tsukamoto H, Harashima S, Kikuchi Y, et al. Infliximab induces potent anti-inflammatory responses by outside-to-inside signals through transmembrane TNF-α. Gastroenterology 2005;128:376–92.

Biased usage of synovial immunoglobulin heavy chain variable region 4 by the anti-glucose-6-phosphate isomerase antibody in patients with rheumatoid arthritis

TAICHI HAYASHI[1], ISAO MATSUMOTO[1,2], TAKANORI YASUKOCHI[1,2], MIZUKO MAMURA[1], DAISUKE GOTO[1], SATOSHI ITO[1], AKITO TSUTSUMI[1] and TAKAYUKI SUMIDA[1]

[1]Division of Clinical Immunology, Major of Advanced Biomedical Applications, Graduate School of Comprehensive Human Science, University of Tsukuba, 1-1-1 Tennodai, Tsukuba, Ibaraki 305-8575; [2]PRESTO, Japan Science and Technology Agency, 4-1-8 Honcho Kawaguchi, Saitama, Japan

Received March 12, 2007; Accepted April 16, 2007

Abstract. Rheumatoid arthritis (RA) is the most common inflammatory arthritis, characterized by marked infiltration of mononuclear cells including B cells into the inflamed synovium. Anti-glucose-6-phosphate isomerase (GPI) antibody (Ab) is an arthritogenic Ab in K/BxN T cell receptor transgenic mice, and is also present in some patients with RA. To characterize synovial B cells from anti-GPI Ab-positive RA, synovial immunoglobulin (Ig) heavy chain variable regions (VH) were compared with those of negative individuals. Synovial tissues were obtained from six RA patients (three anti-GPI Ab-positive and three anti-GPI Ab-negative). Ig-VH genes were amplified by PCR using family-specific primers and were subsequently sequenced. In synovial B cells from anti-GPI Ab-positive RA patients, VH4 and JH4 were predominantly expressed ($p<0.0001$). The immunoglobulin heavy chain complementarity-determining region 3 (IgH-CDR3) length in the synovium of anti-GPI Ab-positive individuals was shorter than that in anti-GPI Ab-negative individuals ($p=0.0005$). In addition, the IgH-CDR3 of anti-GPI Ab-positive patients was rich in basic-ionized amino acids (arginine, histidine, and lysine) near their central position, suggesting a high affinity. Our results support the notion that Ig-VH4 B cells in RA synovium with anti-GPI Ab are affinity-matured and that anti-GPI Ab might be associated with the skewed IgH-CDR3.

Correspondence to: Dr Isao Matsumoto, Clinical immunology, University of Tsukuba, 1-1-1 Tennodai, Tsukuba, Ibaraki 305-8575, Japan
E-mail: ismatsu@md.tsukuba.ac.jp

Abbreviations: -, negative; +, positive; DH, heavy chain diversity regions; FR, framework region; GPI, glucose-6-phosphate isomerase; IgH-CDR3, immunoglobulin heavy chain complementarity determining region 3; JH, heavy chain joining regions; RA, rheumatoid arthritis; SLE, systemic lupus erythematosus; VH, heavy chain variable regions

Key words: autoantibodies, rheumatoid arthritis, glucose-6-phosphate isomerase, B cells, synovium

Introduction

Rheumatoid arthritis (RA) is an inflammatory condition characterized by systemic polyarthritis with bone erosion that affects the peripheral joints. The etiology of RA remains unclear with immunological processes including T cell-B cell interactions, innate immunity, and cytokine activity being implicated (1). In RA, the synovium contains many infiltrating mononuclear cells including B cells at various developmental stages, T cells, and macrophages (2).

Treatments for RA include agents that target cytokines such as tumor necrosis factor. These inflammation-neutralizing approaches have achieved good results in reducing not only joint inflammation but also bone erosion. More recently, depletion of B cells from RA patients has also produced significant therapeutic benefits in several clinical trials (3,4). B cells are thought to be crucial in the pathogenesis of RA, through the production of autoantibodies, antigen presentation, cytokine secretion, and costimulatory signaling. In fact, autoantibodies including rheumatoid factor and anti-cyclic citrullinated peptide antibody (Ab) have been used as diagnostic markers of RA. However, most such autoantibodies are not pathogenic. In contrast, anti-glucose-6-phosphate isomerase (GPI) Ab is a candidate arthritogenic Ab, identified using the K/BxN arthritis model (5-7). In this model, disease development was initiated by the activation of B and T cells. In addition, B cell-deficient mice do not develop arthritis (8). Anti-GPI Ab is also detected in some RA patients, with the reported prevalence varying from 5% to 64% of RA patients (9-12). This Ab is associated with extra-articular manifestations, and its titer correlates with the disease activity (10,13). Moreover, anti-GPI Ab is also detected in the inflamed synovium of RA (14-16). Thus, B cells and autoantibodies appear to play important roles in the pathogenesis of RA in anti-GPI Ab-positive patients, especially in the inflamed joint synovium.

Immunoglobulin molecules are composed of two heavy chains and two light chains, and are characterized by the

Table I. Profile of participating patients (RA1-RA6).

	Age (years)	Sex	Disease duration (years)	Anti-GPI Ab (OD 405 nm) Human	Rabbit	RF (IU/ml)	CRP (mg/dl)	MMP-3 (ng/ml)
RA1	66	F	20	1.78	3.14	156	0.57	363
RA2	70	F	25	2.60	3.47	149	0.42	275
RA3	69	F	16	2.43	2.55	516	3.55	295
RA4	64	F	33	0.72	0.20	78	0.05	ND
RA5	72	F	22	0.62	0.05	119	0.74	215
RA6	74	F	20	0.40	0.36	5	0.56	256

All synovia were from the knees of female patients with rheumatoid arthritis (RA). The cutoff OD was calculated from ELISA reaction of 145 healthy Japanese donors, the mean value + two standard deviation was 1.32 to human recombinant GPI, and 0.94 to rabbit native GPI. Double-positive populations were considered anti-GPI Ab-positive. RA1-3 were anti-glucose-6-phosphate isomerase (GPI) Ab (+), and RA4-6 were anti-GPI Ab (-). Apart from anti-GPI Ab, all other parameters were matched to the utmost extent. GPI, glucose-6-phosphate isomerase; RF, rheumatic factor; CRP, C-reactive protein; MMP-3, matrix metalloproteinase-3; ND, not done.

antigen-binding site sequence and Fc isotype. The antigen-binding site is made up of variable regions and rearranged complementarity-determining regions (CDR) that determine the individual immune properties of any given B cell. The immunoglobulin heavy chain CDR3 (IgH-CDR3) is the most crucial site for antigen binding. H-CDR3 is rearranged by one of 44 variable segments (VH), one or more of 25 diversity segments (DH), and one of six joining segments (JH) (17). In addition, VH genes can be divided into seven sub-families (VH1 to VH7), with overrepresentation of VH4 genes reported in some autoimmune conditions (18). Negative selection of VH4 repertoires is implemented in healthy individuals to avoid autoimmunity (19,20). On the other hand, in RA patients, synovial B cells, especially plasma cells, are also biased to express the VH4 repertoire (21,22), though this was negated in another report (23), and antigen-driven affinity maturation has been reported (23-26).

The present study defined the synovial B cell characteristics of anti-GPI Ab-positive (+) RA patients by analyzing VH regions of synovial B cells from anti-GPI Ab (+) and negative (-) RA patients and compared the rearranged IgH-CDR3 sequences of their VH4 genes. Twenty-seven IgH-VH4 gene sequences from anti-GPI Ab (+) RA patients were compared with thirty-six VH4 gene sequences from anti-GPI Ab (-) patients. In both groups, over 70% of VH4 clones seemed to be undergoing antigen-driven maturation, as evidenced by an R/S ratio of >3 in the CDR and less in the framework region (FR). However, the JH4 gene was more predominant in the synovium of anti-GPI Ab (+) RA patients compared to anti-GPI Ab (-) cases and the lengths of their IgH-CDRs were shorter. In addition, there was no biased usage of VH4 subfamily genes. Together, these findings suggest that B cells from anti-GPI Ab (+) RA synovium are affinity-matured by antigens, with frequent usage of VH4-JH4.

Materials and methods

Subjects. Synovial tissues were obtained from six patients [three were anti-GPI Ab (+) and three were anti-GPI Ab (-)] who satisfied the American College of Rheumatology criteria for RA (1987) (27) (Table I). For selecting anti-GPI Ab-positive patients, enzyme linked immunosorbent assay (ELISA) was performed using two different sources of GPI; a recombinant human GPI (huGPI), and a rabbit muscle GPI (raGPI) (Sigma Chemical Co., St. Louis, MO) which had been described in detail previously (12). Informed consent for using synovial tissues and blood sampling was obtained from all patients at the time of the relevant procedure.

Table II. Specific primers for each VH family.

Internal	
VH1	5'-TCACCATGGACTGCACCTGGA-3'
VH2	5'-CCATGGACACACTTTGCTCCAC-3'
VH3	5'-TCACCATGGAGTTTGGGCTGAGC-3'
VH4	5'-AGAACATGAAACACCTGTGGTTCTT-3'
VH5	5'-ATGGGGTCAACCGCCATCCT-3'
VH6	5'-ACAATGTCTGTCTCCTTCCTCAT-3'
Cγ	5'-CATCGGTCTTCCCCCTGGC-3'
External	
VH1	5'-GAGAAAACCCTGTGAGCACAGCT-3'
VH2	5'-AGTGACTCCTGTGCCCCAC-3'
VH3	5'-GATCAGCACTGAACACAGAGGAC-3'
VH4	5'-GTCATGGACCTCCTGCACAAG-3'
VH5	5'-AGGGCTTCATTTTCTGTCCTCCAC-3'
VH6	5'-GGGGCAGTCACCAGAGCTC-3'
Cγ	5'-GAGCACCTCCGAGAGCACA-3'

Sequences of primers used in nested PCR to detect immunoglobulin heavy chain variable segment (VH) 1-6 family genes.

cDNA synthesis. Synovial tissues were minced and homogenized in Isogen (Nippon Gene, Tokyo, Japan) and extracted with chloroform. RNA was precipitated with isopropanol,

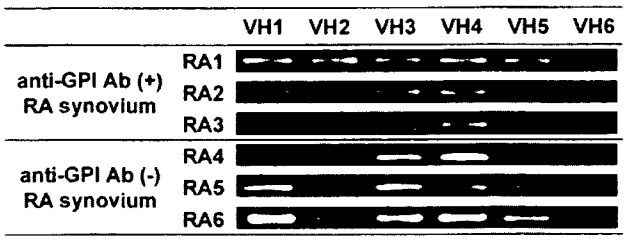

Figure 1. Nested PCR for immunoglobulin heavy chain variable segment (VH) subfamily of rheumatoid synovium. Amplification of VH genes by nested PCR was conducted as shown. Only VH4 genes were amplified in all individuals. VH1 to VH5 were amplified in all cases except RA3.

resuspended in 10 mM Tris·HCl (pH 8.0) and 1 mM EDTA. RevertAid first-strand cDNA synthesis kits (Fermentas, Ontario, Canada) were used for reverse transcription, in accordance with the manufacturer's instructions. Total RNA (5 μg) was used for this reaction.

Amplification of VH genes. Rearranged immunoglobulin VH genes were amplified by PCR. Nested PCR was conducted to obtain sufficient PCR product for electrophoresis. To avoid sequence errors, the first PCR products were subjected to sequencing. Specific oligonucleotides for six different VH families (VH1 to VH6) were used as 5'-primers. Oligonucleotide corresponding to the known Cγ was used as a 3'-primer. For the second PCR, an additional set of primers using the internal sequences was prepared (Table II). One microliter of template was added to 24 μl of a PCR master mix, containing 1.25 U rTaq DNA polymerase (Takara Bio Inc, Shiga, Japan), 2.5 μl of manufacturer's 10X PCR buffer, 2 μl of 2.5 mM dNTPs, and 2.5 μl of each 10-μM primer. The first round of PCR was performed for 25 cycles at 95˚C for 30 sec to denature, 54 or 56˚C for 30 sec to anneal (annealing for VH1, VH2, VH3, VH5 at 56˚C, and for VH4, VH6 at 54˚C), 72˚C for 30 sec to elongate including a previous 5 min of heating at 95˚C to unfold the cDNA, and a final 7-min extension at 72˚C. The second amplification was performed using 1 μl of the first PCR products as templates and the same method as for the first amplification.

Sequence analysis. Aliquots of the first PCR products were separated by electrophoresis using a 1.5% agarose gel, and DNA bands in the range of 400 bp were purified from the agarose gel using a MinElute gel extraction kit (Qiagen, Hilden, Germany). Purified PCR products were cloned into the TA cloning vector (Invitrogen, San Diego, CA). Randomly picked clones were screened for inserts of 400 bp. Positive clones were subjected to cycle sequencing using a BigDye terminator cycle sequence kit (Applied Biosystems, Foster City, CA) according to the manufacturer's recommendations. The sequences were determined by capillary sequencer (Applied Biosystems 310 genetic analyzer). BioEdit (Ibis Therapeutics, Carlsbad, NM) was used for sequence comparison, and JoinSolver [National Institutes of Health, National Institute of Arthritis and Musculosketelal and Skin Diseases (NIAMS) and the Center for Information Technology (CIT)] (28) was used to identify putative Ig-VDJ germline sequences and to clarify the ratio of mutations leading to amino acid replacement to silent mutations (R/S ratio) in the CDR and FR. The IMGT database (Marie-Paule Lefranc, Montpellier, France) was used to confirm the putative Ig-VDJ germline sequences. EMBL Nucleotide Sequence Submissions (European Bioinformatics Institute, Wellcome Trust Genome Campus, Cambridge, UK), and GenBank (National Institutes of Health, Bethesda, Maryland) were also used.

Statistical analysis. The Mann-Whitney U test was used to compare the IgH-CDR3 length of VH between anti-GPI Ab (+) and (-) patients. The two-tailed Fisher exact test was used to determine significant differences in distributions of JH gene usage. Data are expressed as mean ± SD. A p value <0.05 was considered statistically significant.

Results

Amplification of VH family genes. Only VH4 genes were identified from all patients by nested PCR (Fig. 1). VH1 to VH5 genes were also identified except for RA3. In contrast, the amplification of VH6 genes was not sufficient for detection.

R/S ratio. After the first PCR, the VH4 gene products were purified and sequenced. Twenty-seven (17, 8, and 2, respectively) individually rearranged VH4 genes were characterized by sequence analysis in the synovium of anti-GPI Ab (+) RA patients (Table III), and 36 (15, 19, and 2, respectively) were identified in the synovium of anti-GPI Ab (-) individuals (Table III). There was no difference in R/S ratio in the CDR of both groups of VH4 clones [70% (19/27) in anti-GPI Ab (+) and 75% (27/36) in anti-GPI Ab (-)]; the R/S ratio in the CDR was >3, indicating antigen-driven maturation.

VH4 subfamily. Sequences were analyzed by using JoinSolver software to determine the implicated VDJ usage. In the synovium of anti-GPI Ab (+) RA patients, the most frequent VH4 subfamily gene was VH4-59 (12 products) followed by VH4-4 (5 products), VH4-39 (4 products), VH4-31 (3 products), VH4-61 (2 products), and finally, VH4-34 (1 product). In anti-GPI Ab (-) individuals, the dominant detected VH4 subfamily gene was VH4-59 (12 products) followed by VH4-39 (10 products), VH4-31 and VH4-61 (5 products each), and VH4-4 and VH4-34 (2 products each) (Fig. 2a). VH4-39 was therefore relatively less frequent in synovial B cells of anti-GPI Ab (+) RA patients, although the statistical significance was not clear.

JH region. In the synovium of anti-GPI Ab (+) RA patients, the most frequent JH gene was JH4 (19 products) followed by JH3 (3 products), JH6 (2 products), and JH1, JH2, and JH5 (1 product each). In anti-GPI Ab (-) individuals, the most frequent synovial JH gene was JH5 (10 products) followed by JH6 (9 products), JH3 and JH4 (7 products each), and JH2 (3 products) (Fig. 2b). Thus, JH4 usage in synovial B cells of anti-GPI Ab (+) RA patients was 70%, and showed a significantly higher frequency compared to 19% usage in anti-GPI Ab (-) individuals ($p<0.0001$).

IgH-CDR3 characteristics: amino acid composition and IgH-CDR3 length. There was no statistically significant difference